UNIVERSITY of CALIFORNIA

SANTA CRUZ

H I COLUMN DENSITIES, METALLICITIES, AND DUST EXTINCTION OF METAL-STRONG DAMPED Lyα SYSTEMS

A thesis submitted in partial satisfaction of the
requirements for the degree of

BACHELOR OF SCIENCE

in

PHYSICS

by

Kyle F. Kaplan

10 June 2010

The thesis of Kyle F. Kaplan is approved by:

Jason X. Prochaska
Advisor

David P. Belanger
Senior Theses Coordinator

David P. Belanger
Chair, Department of Physics

Abstract

H I Column Densities, Metallicities, and Dust Extinction of Metal-Strong Damped Lyα Systems

by

Kyle F. Kaplan

With the Blue Channel Spectrograph (BCS) on the MMT telescope, we have obtained spectra to the atmospheric cutoff of quasars previously known to show at least one absorption system at $z > 1.6$ with very strong metal lines. We refer to these absorbers as candidate metal-strong damped Lyα systems (cMSDLAs). The BCS/MMT spectra yield precise estimates of the H 1 column densities (N_{HI}) of the systems through Voigt profile analysis of their Lyα transitions. Nearly all of the cMSDLAs (41/43) satisfy the N_{HI} criterion of DLAs, $10^{20.3}$ atoms cm^{-2}. As a population, these systems have systematically higher N_{HI} values than DLAs chosen randomly from quasar sightlines. Combining our N_{HI} measurements with previously measured metal column densities, we estimate metallicities for the MSDLAs. These systems have significantly higher values than randomly selected DLAs; at $z \approx 2$, the MSDLAs show a median metallicity [M/H] ≈ -0.67 that is 0.6 dex higher than a corresponding control sample. This establishes MSDLAs as having amongst the most metal-rich gas in the high z universe. Our measurements extend the observed correlation between Si 2 1526 equivalent width and the gas metallicity to higher values. If interpreted as a mass-metallicity relation, this implies the MSDLAs are the high mass subset of the DLA population. We demonstrate that dust in the MSDLAs reddens their background quasars, with a median shift in the spectral slope of $\delta\alpha = 0.29$. Assuming an SMC extinction law, this implies a median reddening $E_{B-V} \approx 0.025$ mag and visual extinction $A_V \approx 0.076$ mag. The latter quantity yields a dust-to-gas ratio of $log(A_V/N_{\mathrm{HI}}) \approx -22.0$, very similar to estimation for the SMC. Future studies of MSDLAs offer the opportunity to study the extinction, nucleosynthesis, and kinematics of the most chemically evolved, gas-rich galaxies at high z.

Contents

Acknowledgements

1. Introduction

A Damped Lyα Absorption System (DLA) is defined as a neutral hydrogen absorber along a Quasi-Stellar Object (QSO) sight line with an H I column density of $N_{\rm HI} \geq 10^{20.3}$ atoms cm^{-2} (see Wolfe et al. 2005, for a review). DLAs provide an important way to study the gas and dust content of the early universe (e.g. Pettini et al. 1994; Lu et al. 1996; Prochaska & Wolfe 2001). Their heavy elements were synthesized either in nuclear reactions occurring in stellar cores or when massive stars go supernova. Studies of DLAs, therefore, probe the processes of stellar evolution in young galaxies. The large surface density of neutral hydrogen that defines DLAs means these systems contain most of the star forming gas in the early universe (Prochaska et al. 2005; O'Meara et al. 2007). Since the presence of heavy metals in DLAs implies the existence of stars, DLAs likely trace high redshift galaxies along the sight line between the QSO and earth. These high redshift galaxies are thought to be precursors of galaxies like the Milky Way (e.g. Nagamine et al. 2004; Pontzen et al. 2008).

A subset of DLAs exhibit especially strong metal absorption lines. The metal-strong damped Lyα systems (MSDLAs) enable analysis of tens of elements in individual galaxies (Prochaska et al. 2003c). The metal-strong criteria were defined by (Herbert-Fort et al. 2006, ; hereafter, H06) to be absorbers showing ionic column densities that satisfy log N(Zn$^+$)$\geq$13.15 and/or log N(Si$^+$)$\geq$15.95. The MSDLAs, therefore, are absorbers that satisfy the metal-strong criteria and also the DLA criterion on $N_{\rm HI}$. H06 identified a number of MS-DLA candidates from the Sloan Digital Sky Survey (SDSS) and presented higher resolution follow-up spectra of the metal-line transitions. The strong metal absorption lines of these candidates suggests a high metallicity. For many of these MSDLA candidates, however, the Lyα absorption line was bluer than the wavelength coverage in the SDSS spectra, precluding measurements of their H I column densities. Therefore, these absorption systems could not be classified as damped Lyα systems nor could the authors provide metallicity estimates for the gas.

The wavelengths covered by SDSS spectra range from 3800 to 9200 Å (Adelman-McCarthy et al. 2008). This range allows for the identification of DLAs with redshifts corresponding to $z_{\rm abs} \gtrsim 2.2$. For absorbers with $1.5 \lesssim z_{abs} \lesssim 2.2$, the Ly$\alpha$ absorption line lies blueward of the SDSS spectral coverage, but these systems can be observed from ground-based observatories equipped with blue-sensitive spectrometers. With this observational goal in mind, we obtained new spectra from the MMT telescope of various QSO sight lines containing MSDLA candidates using the Blue Channel Spectrograph (BCS).

Here we summarize our classification scheme. Systems with $N_{\rm HI} \geq 10^{20.3}$ atoms cm^{-2} are classified as DLAs. Systems with H I column densities meeting the DLA criteria stated above and with measured metal column densities of log N(Zn$^+$)$\geq$13.15 and/or log N(Si$^+$)$\geq$15.95

are classified as MSDLAs. Candidate MSDLAs are systems identified with strong metal lines in the SDSS spectra (or elsewhere for a few systems) for which there was previously no Lyα coverage and/or no precise measurement of the metal column density. We refer to these candidate MSDLAs as cMSDLAs. Each cMSDLA has had its spectrum taken with the MMT/BCS in order to obtain Lyα coverage.

The gas identified with MSDLAs is analogous to the HI regions found in the Milky Way (e.g. Savage & Sembach 1996). Several heavy elements detected in the gas of MSDLAs are also known to make up interstellar dust in the Milky Way and other nearby galaxies. Dust in the Milky Way is comprised of heavy elements including C, O, Mg, Ni, S, K, Mn, Si, Fe, Al, Ti, and Ca (e.g. Savage & Mathis 1979; Jenkins 2009). Herbert-Fort et al. (2006) presents the abundance ratios of previously observed MSDLAs showing their ratios approach solar. Dust particles preferentially absorb short wavelengths of light, reddening the color of background objects. Ellison et al. (2005) have performed the only extinction estimate for a complete survey of DLAs and set an upper limit to their average reddening of $E_{B-V} < 0.04$ mag. Reddening has been studied in the low redshift universe where nearby galaxies can be well resolved. In contrast, the properties of dust in high redshift galaxies is very poorly constrained. QSO absorption systems provide a probe for studying reddening in high redshift galaxies due to absorption of the QSO's light by the dust in the absorber. A series of studies have been performed on the extinction properties of DLAs beginning several decades ago (e.g. Ostriker & Heisler 1984; Pei et al. 1991). More recently, Murphy & Liske (2004) leveraged the large dataset afforded by SDSS to examine reddening from ≈ 100 DLAs in the SDSS-DR2 using the spectrophotometric observations. Their results show no conclusive evidence for reddening ($E_{B-V} < 0.02$ mag). Reddening in DLAs has also been investigated using the SDSS photometry by Vladilo et al. (2006, 2008), who report evidence for dust. Vladilo et al. (2008) found evidence for reddening when comparing the colors of quasars background to a large sample of DLAs to a control sample of QSOs without DLAs. These authors estititate an average reddening $E_{B-V} \approx 0.006$ mag. Given their large metal column densities, MSDLAs may be expected to show significant reddening.

In this paper we first determine if our candidate MSDLAs meet the DLA and/or the metal-strong criteria and then we search for reddening to see if they contain dust. We cover the observations and data reduction of our candidate MSDLA sample in Section 2. The measurements for redshift and H I column density are given in § 3. We determine metallicities for the cMSDLAs and explore the relationship between [M/H] and the EW of the Si II 1256 line in § 4. Section 5 covers the search for dust reddening and extinction in our data sample and presents the results. We conclude in § 6 with a brief summary.

2. Observations and Reduction

We used the following criteria to select our MSDLA candidates for MMT/BCS spectroscopy, hereafter referred to as cMSDLAs. We selected all SDSS-DR5 quasars with magnitudes $17 < r < 20$ showing 'strong' or 'very strong' Zn II 2026 or Si II 1808 absorption profiles at absorption redshifts $1.6 < z_{abs} < 2.2$. 'Strong' is where the minimum depth of the absorption profile is $\approx 90\%$ the continuum flux, while 'very strong' is when the minimum depth is $\leq 85\%$ the continuum flux. These designations come from visual inspection of the SDSS spectra by JXP and SHF and correspond to the systems with flags 4 for 'strong' or 5 for 'very strong' in the tables of Herbert-Fort et al. (2006). The minimum z_{abs} of the selection is set to ~ 1.6 by the blue atmospheric cutoff, so that Lyα remains accessible at optical wavelengths, while the maximum is set to 2.2 because Lyα becomes accessible in SDSS data directly at higher redshifts. We then gave priority to systems satisfying the metal-strong criterion absorption in higher-resolution follow-up Keck ESI and HIRES spectra (still lacking Lyα coverage), as well as to systems without follow-up data but showing particularly strong metal absorption in the SDSS discovery spectra (at redshifts $1.6 < z_{abs} < 2.2$).

Data on cMSDLAs were acquired over the course of four nights (Sept. 17 2006, Dec. 15 2006, Dec. 16 2006, and Mar. 26 2007) using the MMT telescope at the MMT Observatory on Mt. Hopkins, Arizona. The data were taken with the MMT/BCS using the 800 grooves/mm grating. The slit was $1.25''$ wide giving a spectral resolution of FWHM ≈ 220 km s^{-1}. The wavelengths for these observations range from ~ 3100 to 5100 Å, corresponding to coverage of the Lyα transition for redshifts $1.55 \lesssim z_{abs} \lesssim 3.1$. The observations, totalling 41 QSOs, are summarized in Table 1.

The LowRedux pipeline developed by J. Hennawi, S. Burles, and JXP was used to reduce the MMT data [1]. Standard techniques were used to flat-field and bias subtract the raw MMT data. Objects in the CCD images were traced with a low-order polynomial and extracted optimally. The resulting 1D spectra were calibrated with a composite HeNeAr and HgCd arc lamp spectrum. Instrument flexure was compensated for by shifting the extracted sky spectrum to a template spectrum of the sky convolved with the spectral resolution of the BCS. If more than one spectrum was taken of the same QSO, the multiple exposures were coadded into a single spectrum, weighting by the median S/N ratio of each. The spectra were fluxed using an observation of a spectrophotometric standard star taken on the same night of observation with identical instrumental configuration. The final data products are

---

[1]http://www.ucolick.org/~xavier/LowRedux

Table 1.   List of MMT observations

QSO	RA $J2000$	DEC $J2000$	$Date$ (UT)	$Exposure$ (s)	z_{em}	r $(Mag.)$
J0008-0958	00:08:15.33	-09:58:54.0	2006 Sep 17	1000	2.595	18.38
J0016-0012	00:16:02.40	-00:12:24.9	2006 Dec 14	900	2.087	18.03
J0020+1534	00:20:28.97	+15:34:35.9	2006 Sep 17	1000	1.763	18.79
J0044+0018	00:44:39.32	+00:18:22.7	2006 Dec 14	1200	1.868	18.20
J0058+0115	00:58:14.31	+01:15:30.3	2006 Dec 14	600	2.495	17.69
J0120+1324	01:20:20.36	+13:24:33.6	2006 Sep 17	1000	2.567	19.23
Q0201+36	02:04:55.60	+36:49:18.0	2006 Sep 17	1000	2.912	17.4
J0316+0040	03:16:09.84	+00:40:43.2	2006 Dec 14	1300	2.921	18.66
J0755+2342	07:55:37.22	+23:42:04.7	2006 Dec 16	900	1.825	17.20
J0756+1648	07:56:36.73	+16:48:50.7	2006 Dec 16	1200	2.866	18.76
J0812+3208	08:12:40.68	+32:08:08.6	2006 Dec 16	600	2.704	17.46
J0820+0819	08:20:58.37	+08:19:48.0	2006 Dec 16	900	2.519	18.36
J0831+4025	08:31:08.01	+40:25:31.0	2006 Dec 16	900	2.330	18.87
J0840+4942	08:40:32.95	+49:42:52.8	2006 Dec 16	1200	2.076	19.02
J0856+3350	08:56:18.23	+33:50:42.8	2006 Dec 16	450	1.726	17.18
J0912-0047	09:12:47.59	-00:47:17.4	2006 Dec 16	900	2.859	18.68
J0927+5823	09:27:08.88	+58:23:19.4	2006 Dec 16	900	1.910	18.27
J0938+3805	09:38:46.77	+38:05:49.8	2006 Dec 16	300	1.827	17.13
J0958+4222	09:58:29.47	+42:22:56.8	2006 Dec 16	900	2.656	18.28
J1009+5450	10:09:16.94	+54:50:03.9	2006 Dec 16	900	2.062	19.13
J1019+5246	10:19:39.15	+52:46:27.8	2006 Dec 16	800	2.170	17.92
J1029+1039	10:29:04.15	+10:39:01.5	2007 Mar 25	900	1.795	17.57
J1049-0110	10:49:15.43	-01:10:38.1	2006 Dec 16	720	2.115	17.78
J1054+0348	10:54:00.41	+03:48:01.1	2006 Dec 16	720	2.095	17.98
J1056+1208	10:56:48.69	+12:08:26.8	2006 Dec 16	600	1.923	17.93
J1057+1506	10:57:52.70	+15:06:14.1	2007 Mar 25	1000	2.169	18.06
J1111+1336	11:11:19.10	+13:36:03.8	2007 Mar 25	1000	3.482	17.29
J1224+5525	12:24:38.42	+55:25:14.5	2007 Mar 25	1000	1.879	17.57
J1310+5424	13:10:40.24	+54:24:49.6	2007 Mar 25	1000	1.929	18.50
J1312+5502	13:12:01.09	+55:02:28.6	2007 Mar 25	1500	1.906	19.35
J1341+5818	13:41:44.63	+58:18:17.5	2007 Mar 25	1200	2.054	18.66
J1357+3450	13:57:50.92	+34:50:23.5	2007 Mar 25	1400	2.921	19.03
J1610+4724	16:10:09.42	+47:24:44.5	2006 Sep 16	900	3.217	18.76
J1709+3258	17:09:09.29	+32:58:03.4	2006 Sep 16	600	1.889	19.22
J2100-0641	21:00:25.03	-06:41:46.0	2006 Sep 16	900	3.130	18.17
J2123-0050	21:23:29.46	-00:50:52.9	2006 Sep 16	120	2.262	16.45
J2125+0029	21:25:21.44	+00:29:06.4	2006 Sep 16	900	1.951	19.30
Q2206-19	22:08:51.17	-19:44:06.5	2006 Sep 16	300	2.559	17.0
J2222-0946	22:22:56.11	-09:46:36.2	2006 Sep 16	600	2.926	18.00
J2244+1429	22:44:52.22	+14:29:15.1	2006 Sep 17	700	1.955	18.94
J2340-0053	23:40:23.66	-00:53:27.0	2006 Sep 17	1000	2.085	17.48

*All observed QSO sightlines. This list represents four nights of data. These observations were taken with the MMT BCS using the $800 \frac{grooves}{mm}$ grating. This gives a wavelength coverage of 3100 to 5100Å.

wavelength and flux calibrated 1D spectra. These are publically available online[2].

For the QSOs that have spectra in the SDSS Data Release 6 (Adelman-McCarthy et al. 2008), we compared the SDSS and MMT spectra visually as a consistency check on our data reduction. When comparing the MMT spectra to the SDSS spectra, the relative flux of the MMT spectra did not always match the flux of the SDSS spectra. We take the SDSS fluxing to be correct and scaled the flux of our MMT spectra correspondingly. The correction was a simple multiplicative scalar; we estimate that the relative fluxing of the MMT is accurate to $\approx 10\%$. This scaling process is further elaborated upon in our discussion on searching for reddening by MSDLAs in Section 5.

While comparing the MMT spectrum to the SDSS spectrum from the years 2006.96 and 2002.18 of cMSDLA J1054+0348, two blueshifted broad absorption line features appeared in the newer MMT spectrum in the that were not present in the older SDSS spectrum. The time between observations was 4.78 years. This serendipitous discovery is the first observation of a high redshift QSO where associated absorption lines were observed to appear (Hamann et al. 2008). These absorption lines signify the appearance of a high velocity outflow in the QSO along the line of sight.

No other variable absorption features were identified in the spectra.

3. Determination of $N_{\rm HI}$ column densities from DLA Lyα absorption

The principal motivation for the observations analyzed here was to measure the H I column densities of $z < 2.2$ cMSDLAs. The MMT observations provide spectral coverage of the previously unobserved Lyα transition. With these data, $N_{\rm HI}$ values can be estimated from line-profile fits to the Lyα lines (e.g. Prochaska et al. 2005). These $N_{\rm HI}$ values are required to establish the gas metallicity and to verify that a system satisfies the DLA criterion. The cMSDLAs which satisfy both the DLA criterion ($\log N_{\rm HI} \geq 20.3$) and metal-strong criterion (H06) are then classified as MSDLAs.

The Lyα lines were analyzed using the program x_fitdla from the XIDL package[3]. For completeness, we considered all Lyα lines in our dataset with equivalent widths exceeding ≈ 5Å, independent of whether the system was a cMSDLA. For two of the cMSDLAs in our MMT sample (J1111+1336 and J2100−0641) whose redshifts exceed $z_{abs} > 3.1$, the Lyα
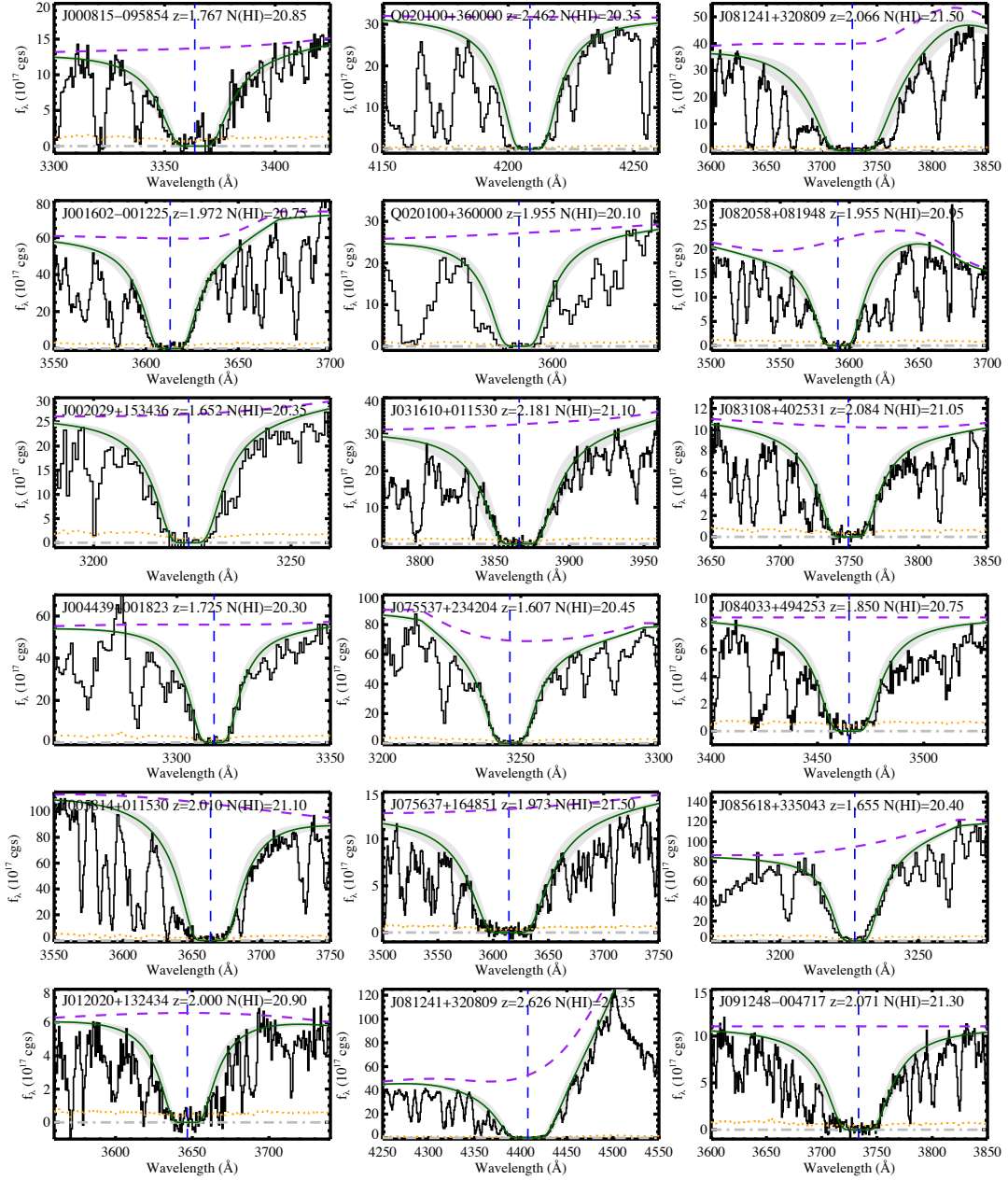
---

[2]http://www.ucolick.org/~xavier/DLA/MSDLA

[3]http://www.ucolick.org/~xavier/IDL

Fig. 1.— Enlargement of the Lyα transition for every strong absorber (equivalent width exceeding ≈ 5Å) identified in our MMT spectra. Overplotted on the data is a model of the best-fit Voigt profile with the redshift and N_{HI} value (Table 2) listed in each panel. The shaded region indicates an estimate for the uncertainty, corresponding to ≈ 90% confidence. The dotted (orange) line traces the 1σ error array and the horizontal dashed (purple) line is our best estimate for the quasar continuum flux. [See the end of this manuscript for all the fits.]

absorption feature was redshifted past our wavelength coverage. This is because we were searching for molecular hydrogen in these QSOs (see Section 4). These DLAs were analyzed using spectra from the SDSS DR6 instead. A total of 49 possible DLAs were identified, that includes serendipitous DLAs along the sightlines (i.e. ones that were not targeted as MSDLA candidates). Redshifts for each DLA were estimated from the centroids of corresponding low-ion metal transitions, with preference given to the O I 1302 transition as listed in Table 2.

With the redshift of the possible DLA constrained, we measured the H I column density as follows. First, the continuum from the background QSO is modeled by hand in the region local to the Lyα line. The centroid of the Lyα line is given by the previously measured redshift. Then a Voigt profile is fit to the Lyα absorption feature by visual inspection. The value of log N_{HI} is adjusted until the wings of the profile best fit the observed Lyα line. The continuum and $N_{\rm HI}$ values were then iteratively modified (generally by $< 10\%$ from our initial guess) until an optimal match to the data was established. The resulting profile gives the H I column density directly. All of the $N_{\rm HI}$ values are listed in Table 2. The errors in these values are dominated by systematic uncertainties, primarily continuum placement and line-blending in the damped wings of the Voigt profile. In all cases, we assumed a minimum error of 0.15 dex. We estimate larger uncertainties for DLAs where the QSO continuum is especially challenging, there is significant emission-line contamination from the QSO and/or if there is substantial line-blending with the Lyα forest. All of our Voigt profile fits are presented in Fig. 1.

We have compared our values with existing estimates from the literature. Previous measurements of H I column densities were found for eight of the absorption systems we observed. Four of these previous measurements from the literature were made at significantly higher spectral resolution (Prochaska & Wolfe 1996; Prochaska et al. 2003b, 2001). We have adopted these H I column density measurements over our own (see fourth column of Table 2). In all cases the difference is well within our estimated error. We caution, however, that because the uncertainties are dominated by systematic error that are largely independent of the spectral resolution and signal-to-noise, the good agreement does not mean that we have overestimated the uncertainties (see also Prochaska et al. 2005).

We targeted 43 systems as cMSDLAs, most of which had no prior H I column density measurements. Beyond the 43 absorption systems targeted, five QSO slight lines contain a second absorption system. This brings the total amount of Lyα absorbers to 49. Out of the 49 Lyα absorption systems identified, 42 have H I column densities that satisfy the DLA criterion (log $N_{HI} \geq 20.3$ atoms cm^{-2}). The remainder are super Lyman limit systems (SLLS) with log $N_{\rm HI} \geq 19$. All but two of the cMSDLAs are confirmed as damped Lyα systems. The two SLLS that were also cMSDLAs (J2123$-$0050 at $z_{\rm abs} = 2.058$ and J1009+5450 at

Table 2.   MMT Sample of DLA Candidates

QSO	z_{abs}	$\log N_{\rm HI}^a$ (cm^{-2})	$\log N_{\rm HI}^b$ (cm^{-2})	[M/H]^c	W_{1526}^d (Å)	cMSDLA?	MSDLA?^{e}
J000815.33-095854	1.768	20.85 ± 0.15	20.85 ± 0.15	-0.28 ± 0.15	1.38 ± 0.10	Yes	Yes
J001602.40-001225	1.970	20.75 ± 0.15	20.83 ± 0.07	-0.86 ± 0.13	2.46 ± 0.10	Yes	No
J002028.96+153436	1.653	20.35 ± 0.15	20.35 ± 0.15	-0.51 ± 0.17	0.88 ± 0.13	Yes	No
J004439.32+001822	1.725	20.30 ± 0.15	20.30 ± 0.15	-0.66 ± 0.12	0.89 ± 0.08	Yes	No
J005814.31+011530	2.010	21.10 ± 0.15	21.10 ± 0.15	-0.99 ± 0.16	1.33 ± 0.05	Yes	No
J012020.37+132433	1.999	20.90 ± 0.15	20.90 ± 0.15	-0.56 ± 0.16	0.79 ± 0.14	Yes	No
Q0201+36	1.955	20.10 ± 0.15	20.10 ± 0.15		...	No	...
Q0201+36	2.463	20.35 ± 0.15	20.38 ± 0.05	-0.36 ± 0.05	...	Yes	No
J031609.83+004043	2.180	21.10 ± 0.20	21.10 ± 0.20	-1.20 ± 0.22	0.62 ± 0.02	Yes	No
J075537.22+234204	1.670	20.45 ± 0.15	20.45 ± 0.15		...	Yes	...
J075636.73+164850	1.973	21.50 ± 0.15	21.50 ± 0.15		...	Yes	...
J081240.68+320809	2.626	21.35 ± 0.15	21.35 ± 0.10	-0.88 ± 0.11	...	Yes	Yes
J081240.68+320809	2.067	21.50 ± 0.20	21.50 ± 0.20	-1.83 ± 0.20	...	No	No
J082058.37+081948	1.955	20.95 ± 0.15	20.95 ± 0.15		1.07 ± 0.07	Yes	...
J083108.01+402531	2.084	21.05 ± 0.15	21.05 ± 0.15		1.56 ± 0.08	Yes	...
J084032.96+494252	1.851	20.75 ± 0.15	20.75 ± 0.15	-0.43 ± 0.17	1.58 ± 0.13	Yes	No
J085618.23+335042	1.655	20.40 ± 0.15	20.40 ± 0.15		0.62 ± 0.05	Yes	...
J091247.59-004717	2.071	21.30 ± 0.15	21.30 ± 0.15	-0.89 ± 0.16	...	Yes	Yes
J092708.88+582319	1.635	20.40 ± 0.25	20.40 ± 0.25	-0.22 ± 0.25	1.92 ± 0.15	Yes	No
J093846.77+380549	1.827	19.75 ± 0.15	19.75 ± 0.15		...	Yes	...
J095829.47+422256	1.853	20.90 ± 0.15	20.90 ± 0.15		...	Yes	...
J095829.47+422256	2.065	20.95 ± 0.15	20.95 ± 0.15		1.24 ± 0.06	Yes	...
J100916.94+545003	1.623	20.20 ± 0.15	20.20 ± 0.15		0.83 ± 0.13	Yes	...
J100916.94+545003	1.892	21.65 ± 0.15	21.65 ± 0.15		1.12 ± 0.11	Yes	...
J101939.15+524627	1.833	19.45 ± 0.15	19.45 ± 0.15		...	No	...
J101939.15+524627	2.018	20.35 ± 0.15	20.35 ± 0.15		1.13 ± 0.05	Yes	...
J102904.15+103901	1.622	21.10 ± 0.25	21.10 ± 0.25		1.21 ± 0.07	Yes	...
J104915.43-011038	1.658	20.35 ± 0.15	20.35 ± 0.15	-0.09 ± 0.15	1.74 ± 0.07	Yes	No
J105400.41+034801	2.068	20.40 ± 0.35	20.40 ± 0.35		1.02 ± 0.06	Yes	...
J105648.69+120826	1.609	21.45 ± 0.15	21.45 ± 0.15	-0.43 ± 0.23	1.19 ± 0.09	Yes	Yes
J105752.70+150614	1.865	19.35 ± 0.15	19.35 ± 0.15		...	No	...
J105752.70+150614	2.076	20.50 ± 0.15	20.50 ± 0.15		1.41 ± 0.07	Yes	...
J111119.10+133603	3.201	21.25 ± 0.15	21.25 ± 0.15		...	Yes	...
J122438.42+552514	1.673	20.40 ± 0.15	20.40 ± 0.15		0.81 ± 0.04	Yes	...
J131040.24+542449	1.600	20.25 ± 0.25	20.25 ± 0.25		0.57 ± 0.16	No	...
J131040.24+542449	1.801	21.45 ± 0.15	21.45 ± 0.15	-0.51 ± 0.15	0.84 ± 0.12	Yes	Yes
J131201.09+550228	1.860	21.20 ± 0.25	21.20 ± 0.25		2.23 ± 0.27	Yes	...
J134144.63+581817	1.741	21.00 ± 0.15	21.00 ± 0.15		1.79 ± 0.08	Yes	...
J135750.92+345023	2.132	20.45 ± 0.25	20.45 ± 0.25		...	Yes	...
J161009.42+472444	2.508	21.00 ± 0.15	21.00 ± 0.15	-0.10 ± 0.15	1.76 ± 0.09	Yes	Yes
J170909.28+325803	1.830	20.95 ± 0.15	20.95 ± 0.15	-0.28 ± 0.15	1.62 ± 0.15	Yes	Yes
J210025.03-064146	3.092	21.05 ± 0.15	21.05 ± 0.15	-0.67 ± 0.15	1.09 ± 0.04	Yes	No
J212329.46-005052	2.058	19.45 ± 0.15	19.45 ± 0.15		0.48 ± 0.03	Yes	...
J212521.44+002906	1.751	21.35 ± 0.20	21.35 ± 0.20		1.71 ± 0.23	Yes	...
Q2206-19	1.920	20.65 ± 0.15	20.65 ± 0.07	-0.37 ± 0.07	0.99 ± 0.01	Yes	No
Q2206-19	2.076	20.50 ± 0.15	20.43 ± 0.06	-2.26 ± 0.07	...	No	No
J222256.11-094636	2.354	20.55 ± 0.15	20.55 ± 0.15	-0.61 ± 0.16	1.20 ± 0.06	Yes	No
J224452.22+142915	1.816	20.70 ± 0.15	20.70 ± 0.15	-0.59 ± 0.16	1.08 ± 0.13	Yes	No
J234023.66-005327	2.055	20.35 ± 0.15	20.35 ± 0.15	-0.59 ± 0.15	...	Yes	No

^{a}Measured from our MMT observations.

^{b}Adopted value based on comparison of our measurement with ones in the literature (see text).

^{c}Logarithmic metallicity relative to solar as measured from ionic transitions of Zn$^+$, Si$^+$, or S$^+$. The measurements adopt the solar abundances of Asplund et al. (2009).

^{d}Rest-frame equivalent width of the Si II 1526 transition. In nearly every case, this was measured from a Gaussian fit to the observed line in the SDSS spectrum. The remainder are boxcar integrations of higher resolution observations.

^{e}DLAs without an entry have not been observed at sufficiently high spectral resolution to test the metal-strong criteria. Entries that are cMSDLA and have $\log N_{\rm HI} \geq 20.3$ but are not MSDLAs have metal column densities below the metal-strong criteria.
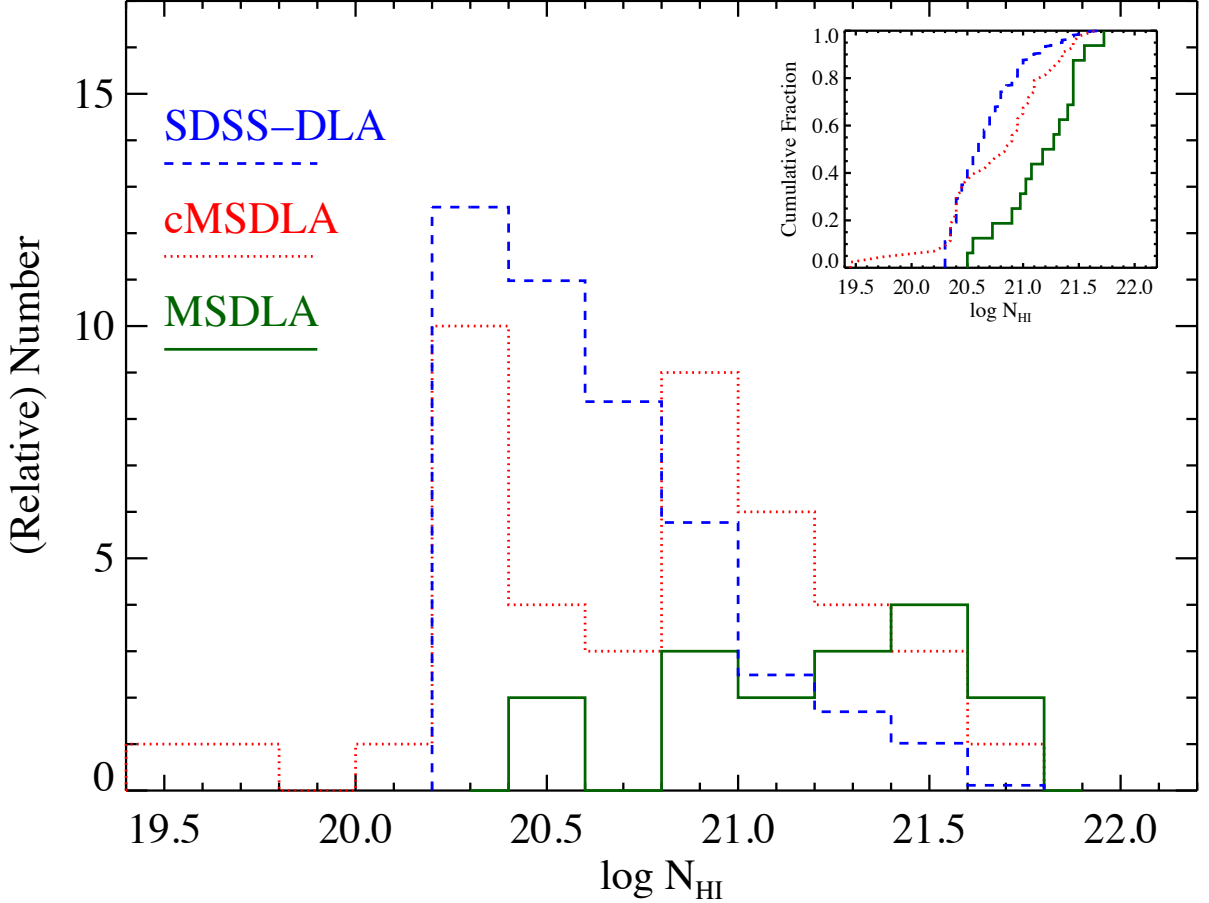
Fig. 2.— Histogram comparing the H I column densities of the MSDLA candidates (cMS-DLA; red, dotted), confirmed MSDLAs (MSDLA; green, solid), and a comparison sample (blue, dashed) of $z < 3$ DLAs from Data Release 5 of the Sloan Digital Sky Survey (SDSS-DLA Prochaska & Wolfe 2009). The SDSS histogram (scaled to have identical area under the curve as the cMSDLA histogram) represents the distribution of $N_{\rm HI}$ values for randomly selected quasar sightlines at $z \sim 3$ and serves as a control sample. A normalized cumulative plot is shown in the top right corner. The cMSDLA and especially the confirmed MSDLA exhibit significantly higher $N_{\rm HI}$ value on average. A Kolmogorov-Smirnov test comparing the cMSDLA and MSDLA against the SDSS control sample gives KS probabilities of $P_{KS} = 0.002$ and 10^{-5} respectively.

$z_{abs} = 1.623$) may represent new examples of super-solar Lyman limit systems (e.g. Péroux et al. 2006; Prochaska et al. 2006).

Figure 2 shows a histogram of H I column densities for MSDLAs, our sample of cMSD-LAs, and a comparison sample of randomly selected DLAs from the SDSS-DR5 (Prochaska & Wolfe 2009). The latter sample contains 380 DLAs with $z_{abs} = [2.2, 3.0]$. Although the median redshift of this control sample is higher than metal-strong systems, Prochaska & Wolfe (2009) have demonstrated that evolution in the shape of the H I frequency distribution is weak for DLAs. The MSDLAs and cMSDLAs show systematically higher H I column densities then the comparison sample. Formally, a two-sided KS test yields probabilities $P_{KS} = 0.002, 10^{-5}$ that cMSDLAs and MSDLAs respectively are drawn from the same parent population as the control sample. This is consistent with the expectation that selecting systems with high metal column densities will select systems with high H I column densities.

4. Metal Column Density and Metallicity Measurements

To estimate the metallicities of the MSDLAs we simply compare the measured H I column density with the ionic column density of an element expected to trace the metal abundance of the system. Generally, one avoids refractory elements like Fe because these can be depleted from the gas-phase and may give systematically low metallicity values. Previous work has focused on low-ion transitions of Si, S, and Zn which are mildly refractory, give similar results, and have several low-ion transitions for analysis (e.g. Prochaska & Wolfe 2001; Prochaska et al. 2003a). Unfortunately, the MMT and SDSS spectra have insufficient spectral resolution for a precise column density measurement. Therefore, we have adopted the ionic column densities for these DLAs from previous works (H06; Prochaska et al. 2007) and new Keck/HIRES observations that will be presented in a future paper (Prochaska et al., in prep.). Measurements of metal column densities exist for 24 of the absorbers in our sample, 22 of which are cMSDLAs. These metal column density measurements test whether a cMSDLA satisfies the metal-strong criteria set by H06: $\log N(Zn^+) \geq 13.15$ and/or $\log N(Si^+) \geq 15.95$. Those cMSDLAs that meet the metal-strong criteria are classified as MSDLAs. Out of 22 cMSDLAs with metal column density measurements, 7 meet the metal-strong criteria and are classified as MSDLAs. When combined with measurements from the literature, we have a total sample of 15 MSDLAs with $z_{abs} \geq 1.60$.

The metallicity of a DLA is usually expressed as the logarithmic ratio of the metal to H I column densities relative to the solar abundance, [M/H]. Here, the letter 'M' refers to metallicity, derived from one of the elements listed above. For the solar abundance scale, we adopt the compilation of (Asplund et al. 2009) using meteoritic values when available
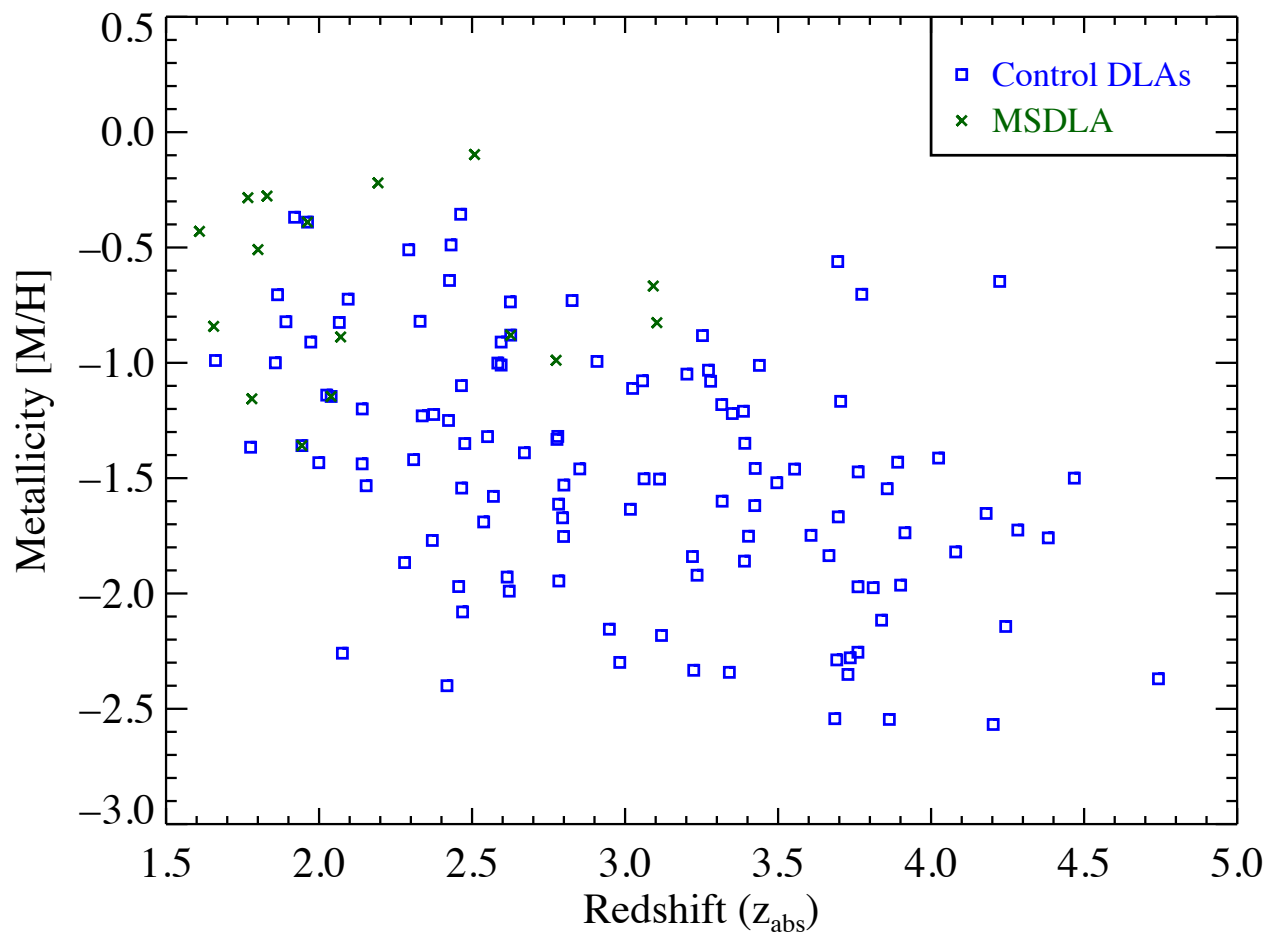
Fig. 3.— Scatter plot of gas metallicity ([M/H]; determined from Si, S, O, or Zn) against absorber redshift. The blue squares show the metallicity values for a (nearly) random DLA sample (Prochaska et al. 2003a) and the (green) x's show values for the MSDLA systems. We find that the MSDLA systems exhibit systematically higher metallicity than the random sample to at least $z \approx 3$.

excepting C, N, and O. The values are listed in Table 2. These new metallicity values allow investigation of several relationships. In the universe, metallicity increases over time from the original abundances created in Big Bang nucleosynthesis as stars evolve and die enriching their surrounding interstellar media. One would expect that metallicities of DLAs to decrease with greater lookback time (here quantified by increasing absorber redshift). In Fig. 3, the metallicity of the DLAs is compared with the absorber's redshift. The DLAs from Prochaska et al. (2003a), which are taken as a random sample, follow the expected trend. The MSDLAs exhibit systematically higher metallicity than the random sample over the range of redshifts covered. Specifically, we measure a median metallicity for the MSDLA of $[\mathrm{M/H}] = -0.67$ dex over the redshift interval $z_{\mathrm{abs}} = [1.6, 3.1]$ and calculate a median $[\mathrm{M/H}] = -1.32$ dex from the control sample over the same interval. We expect this result since the MSDLAs are selected for their high metal column densities, which should select systems with high metallicities across a range of redshifts.

DLAs, by definition, contain a large amount of neutral hydrogen. It can be expected that some might also contain large amounts of molecular hydrogen (H_2), especially if the QSO sight-line probes a high density region of the DLA. H_2 has been detected in DLAs by previous authors (e.g. Ge & Bechtold 1997; Petitjean et al. 2000). Three of the cMSDLAs show evidence of H_2 in their spectra. These systems are J0812+3208 ($z_{\mathrm{abs}} = 2.626$), J2100−0641 ($z_{\mathrm{abs}} = 3.092$), and J2340−0053 ($z_{\mathrm{abs}} = 2.054$). The remainder of the systems show no obvious H_2 absorption at the strong transitions of the $J = 0$ and $J = 1$ levels (i.e. $N(H_2) < 10^{17}$ atoms cm^{-2}). We conclude that only 3 out of the 32 systems have significant H_2 absorption giving a detection rate of $\approx 10\%$. This is a surprisingly low detection rate given that the systems have systematically higher metallicity than random samples of DLAs. Indeed, Noterdaeme et al. (2008) report a detection rate of $\approx 35\%$ for systems with $[\mathrm{M/H}] \geq -1.3$ to a similar limit on $N(H_2)$. The incidence is higher (2 of 6 for systems with good coverage of the Lyman-Werner transitions) if we restrict the discussion to MSDLAs, but this sample is too small for statstical discussion.

Figure 4 compares the metallicity of DLAs to their H I column densities (N_{HI}) for the MSDLAs and cMSDLAs along with the same random sample (Prochaska et al. 2003a). Most of our confirmed MSDLAs lie on or beyond the upper bound on metallicity/N_{HI} discussed by Boisse et al. (1998), who suggested this upper bound is caused by obscuration of the background QSO by large amounts of dust. In fact, MSDLAs must by definition be near or above this upper bound. Our observations of MSDLAs clearly lie beyond this limit, indicating that dust does not always completely obscure systems with very high metal column densities (see also H06). This lends further support to prior assertions that this observational bound was not driven entirely by obscuration (Ellison et al. 2005; Krumholz et al. 2009). The consistently higher metallicity of MSDLAs could incidate that their sightlines probe regions
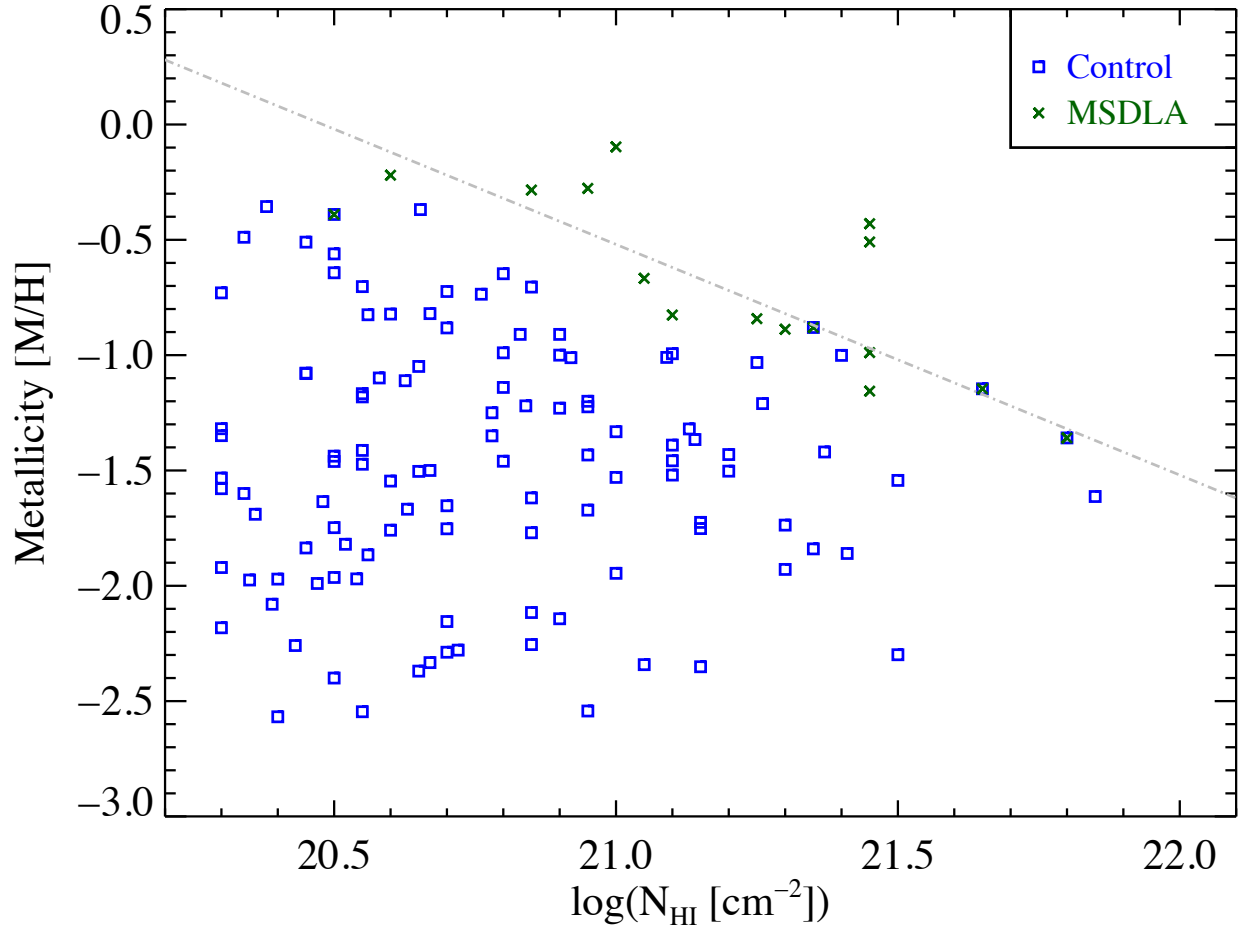
Fig. 4.— Scatter plot of gas metallicity ([M/H]; determined from Si, S, O, or Zn) against absorber N_{HI} value, restricted to those exceeding the damped Lyα criterion. The blue squares show the metallicity values for a (nearly) randomly selected DLA sample (Prochaska et al. 2003a) and (green) x's show values for the MSDLA systems. The overplotted dash-dot line traces the 'upper-bound' to the [M/H], N_{HI} distribution analyzed by Boisse et al. (1998). The MSDLA, by definition, follow or exceed this supposed boundary. Our results indicate that dust obscuration does not entirely preclude the detection of sightlines with very high metal column density.

near the center of galaxies (or proto-galaxies) if a radial gradient in metallicity exists for high z galaxies. Alternatively, the higher metallicity may indicate that MSDLAs probe more chemically evolved systems and, if a mass-metallicity relation holds at high z (e.g. Erb et al. 2006; Prochaska et al. 2008), higher mass galaxies.

To test the latter hypothesis, we examined the relation between Si II 1526 equivalent width W_{1526} and the gas metallicity. A random sample of DLAs was shown by Prochaska et al. (2008) to exhibit a correlation between these two measures, which the authors interpret as a mass-metallicity relation (see also Murphy et al. 2007). The key point is that W_{1526} is dominated by the kinematics of the gas, generally weaker 'clouds' that contribute little to the column density of Si^+. More massive systems have higher gravitational potentials, thus faster rotational and/or virial motion which leads to a greater broadening of Si II 1526. W_{1526} values for the systems in this sample have been measured using Keck HIRES and ESI spectra by (H06; Prochaska et al. 2007) and Kaplan et al. (in prep). These metal-strong systems probe a higher range of metallicities than previous observations, extending the W_{1526} vs. [M/H] relation. Figure 5 shows this relationship for our data and a random sample of DLAs with lower metallicities taken from Prochaska et al. (2003a).

Our new measurements indicate the W_{1526}-metallicity relationship holds to solar metallicity with roughly constant scatter. If there is an underlying mass-metallicity relationship then the MSDLAs, with their systematically higher metallicities, also represent the subset of DLAs with highest mass. These are ideal candidates for follow-up imaging surveys if one wishes to maximize observing efficiency (Möller et al. 2004).

5. Dust Extinction

Dust in the Galaxy's interstellar medium is known to absorb and scatter the light from background objects. Dust consists of grains of heavy elements that have solidified out of the atmospheres of cool stars and the interstellar medium. MSDLAs, with their high metal column densities, make good candidates to search for dust in the high redshift universe and set (rare) constraints on the properties of such dust, e.g. the dust-to-metals ratio, extinction laws.

This absorption is most efficient at short wavelengths, and has the tendency to redden the color of the background light source. This process is known as extinction and approximately follows a λ^{-1} relation. In the case of QSO absorption systems like DLAs, dust in the DLA reddens the color of the background QSO. Extinction (A_λ) is defined as the change in magnitude due to dust absorption. Reddening is the difference in extinction between two
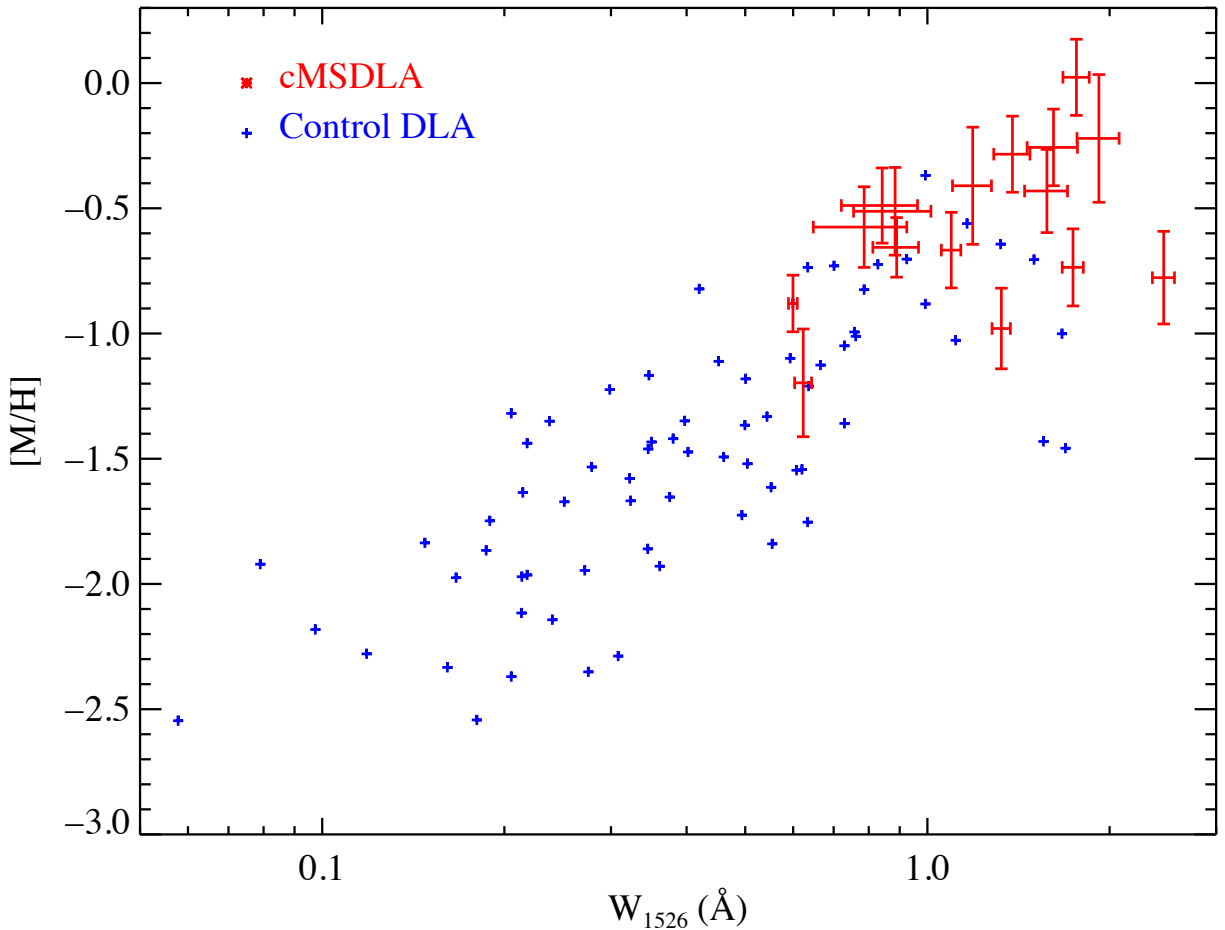
Fig. 5.— Gas metallicity values versus rest-frame equivalent width of the Si II 1526 transition (W_{1526}) as measured for the random sample of DLAs from Prochaska et al. (2003a) and our MSDLA candidates. Our new observations indicate that the $[M/H]/W_{1526}$ correlation holds to nearly solar metallicity and very large W_{1526} values. If interpreted as a mass-metallicity relation (Prochaska et al. 2008), this implies the MSDLAs represent the most massive galaxies of the DLA population. Errors for the contorl DLAs are negligible for W_{1526} and are $0.1 - 0.15$ dex for the $[M/H]$ values.

bands, most commonly reported between B and V as $E_{B-V} \equiv A_B - A_V$.

Extinction in a large sample of DLAs from the SDSS have been studied photometrically. Vladilo et al. (2008) found evidence for reddening in a large sample of DLAs when compared to QSOs that contain no absorbers. Previously, Vladilo et al. (2006) found evidence for reddening in 5 out of 13 DLAs selected to have strong Zn II absorption lines. Several of these 5 systems qualify as MSDLAs. In fact two are also in our sample of MSDLA candidates (J0016$-$0012 and J2340$-$0053) and both show evidence of reddening. The high metal column densities in MSDLAs suggest that they may contain a large amount of dust. If photometric studies of DLAs find evidence for dust in two systems that are metal strong candidates, it is plausible that many more cMSDLAs will also yield evidence for dust.

5.1. Quasar Power-Law Slopes

In principle, analysis of spectrophotometric observations for reddening are ideal because the extinction can be explored as a function of wavelength. In practice, this is difficult because the intrinsic shape of the background QSO continuum is unknown and is likely to vary with significant scatter. While this makes constraining reddening for individual systems difficult, one may explore systematic shifts in the overall population by essentially averaging over the scatter in intrinsic QSO continua. A spectroscopic search for reddening in DLAs was previously conducted by Murphy & Liske (2004) who fit a power-law ($f_\nu \propto \nu^\alpha$) to the QSO continuum for each system and compared the exponent α to a control sample of QSOs. These DLAs were not selected to be metal strong, and the authors did not detect reddening along the 70 DLA sightlines. We now conduct the same type of analysis, but with our sample of cMSDLAs.

The typical QSO spectrum in the optical and ultraviolet consists of two distinct features. The continuum spans across all wavelengths and is shaped by one or more power-laws (e.g. Telfer et al. 2002). Broad emission lines, such as Lyα, lie on top of the continuum. Our spectra of cMSDLAs taken with the MMT/BCS covers a wavelength range of $\sim$ 3100 to 5100Å, the blue end of the visible spectrum. Most of the cMSDLAs also have corresponding SDSS DR6 spectra, covering a wavelength range of $\sim$ 3800 to 9200 Å. Both the MMT and SDSS spectra provide a wide coverage of wavelengths spanning the UV spectrum in the QSO rest-frame.

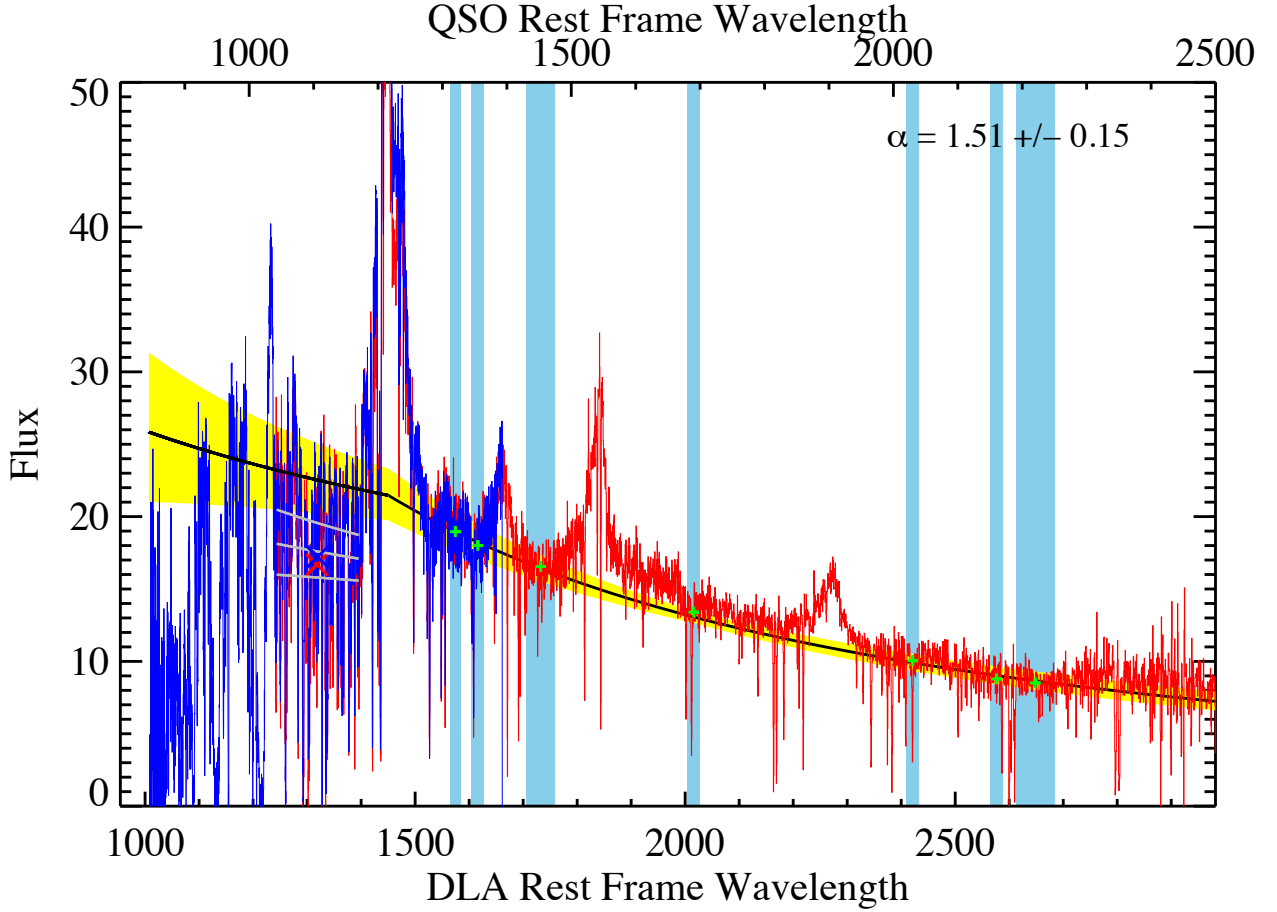The first step in this analysis is to model the QSO's continuum spectrum by fitting a

Fig. 6.— SDSS (red; $\lambda_{QSO} > 800$Å) and MMT (dark blue; $\lambda_{QSO} < 1200$Å) spectra of the quasar J0958+4222 ($z_{em} =2.656$). The upper x-axis shows the wavelengths in the quasar rest-frame while the lower x-axis refers to the rest-frame of the foreground candidate metal-strong damped Lyα system (cMSDLA; $z_{abs} =2.065$). The vertical shaded regions indicate 'emission-free' windows in the quasar continuum, which were used to model a power-law spectrum $f_\lambda \propto \lambda^{-\alpha}$ to the SDSS data. The (green) plus signs show the median flux in each region. The black solid line shows the best-fit model, normalized at $\lambda_{QSO} = 1700$Å and the yellow shaded region about the line indicates the 1σ uncertainty. A second power-law, with an exponent that differs by $\Delta\alpha = 1.0$, describes the model quasar continuum blueward of $\lambda_{QSO} = 1216$Å. The short, grey lines at $\lambda_{QSO} \approx 1100$Å show the predicted mean flux (and the uncertainty) of the continuum when accounting for absorption by the Lyα forest (Kirkman et al. 2005). The X's show the mean flux for the MMT (blue) and SDSS (red) spectra in the region indicated by the grey lines.

power-law to the regions in the spectrum free from QSO emission lines:

$$f_r(\lambda) = f_{obs}(1700\text{Å}) \left(\frac{\lambda}{1700\text{Å}} \right)^{-\alpha}. \tag{1}$$

See Fig. 6 for an example of our power-law model. This is based on a similar method created by Murphy & Liske (2004). The seven 'emission free' (EM-free) regions are 1312-1328, 1345-1365, 1430-1475, 1680-1700, 2020-2040, 2150-2170, and 2190-2250 Å in the QSO rest frame. We mask emission-free regions which are unreliable or contaminated by absorption lines from the DLA. The median flux and central wavelength in each emission free region form points from which the power-law curve is fitted. We normalize our power-law fit to the QSO's flux at 1700 Å. This fit is done in the SDSS spectrum because the fluxing is presumed to be accurate and the SDSS spectrum covers longer wavelengths redward of the QSO's Lyα line where the Lyα forest cannot contaminate the continuum flux. We derived a statistical error on α using the IDL program 'curvefit.' These ranged from from approximately $1-50\%$ in α. It is evident from inspection of the data and model that these are frequently poor estimates of the total uncertainty. We estimate the total uncertainty (statistical and systematic) to be $15-20\%$.

The exponent of the power-law (α) presumably becomes depressed when the background QSO is reddened by dust. The analysis by Murphy & Liske (2004) could not find any significant difference between the exponents for ordinary non-metal strong DLAs and a control sample of QSOs. The same comparison is done using our sample of cMSDLAs, as seen in Fig. 7. (Table 3). For each cMSDLA, we construct a control sample of ~ 12 randomly selected QSOs with a similar redshift (Δz_{abs}=0.2) and r-magnitude (Δr=0.355 mag). The latter value was chosen to give at least 12 systems in the control sample for each cMSDLA. The cMSDLA sample exhibits systematically lower α then the combined control sample, indicating they are reddening their background quasars. This is true for both median (see below) and mean statistics indicating there is reddening by the bulk of the cMSDLAs. This contrasts with the results from Murphy & Liske (2004) who found no conclusive evidence for reddening in 'random' DLAs. The difference in the median exponent of the control sample α_C and the median exponent of the cMSDLAs α_m is defined to be $\delta\alpha \equiv \alpha_C - \alpha_m$. We measure $\alpha_C = 1.45$ and $\alpha_m = 1.16$ giving $\delta\alpha = 0.29$. In the following section we use $\delta\alpha$ to constrain the typical extinction and reddening by dust in these systems.

5.2. Constraining the Extinction and Reddening

The value of $\delta\alpha$ found in the previous section indirectly reveals the average flux absorbed by the cMSDLAs sample via dust reddening. In this section we use $\delta\alpha$ to estimate the average
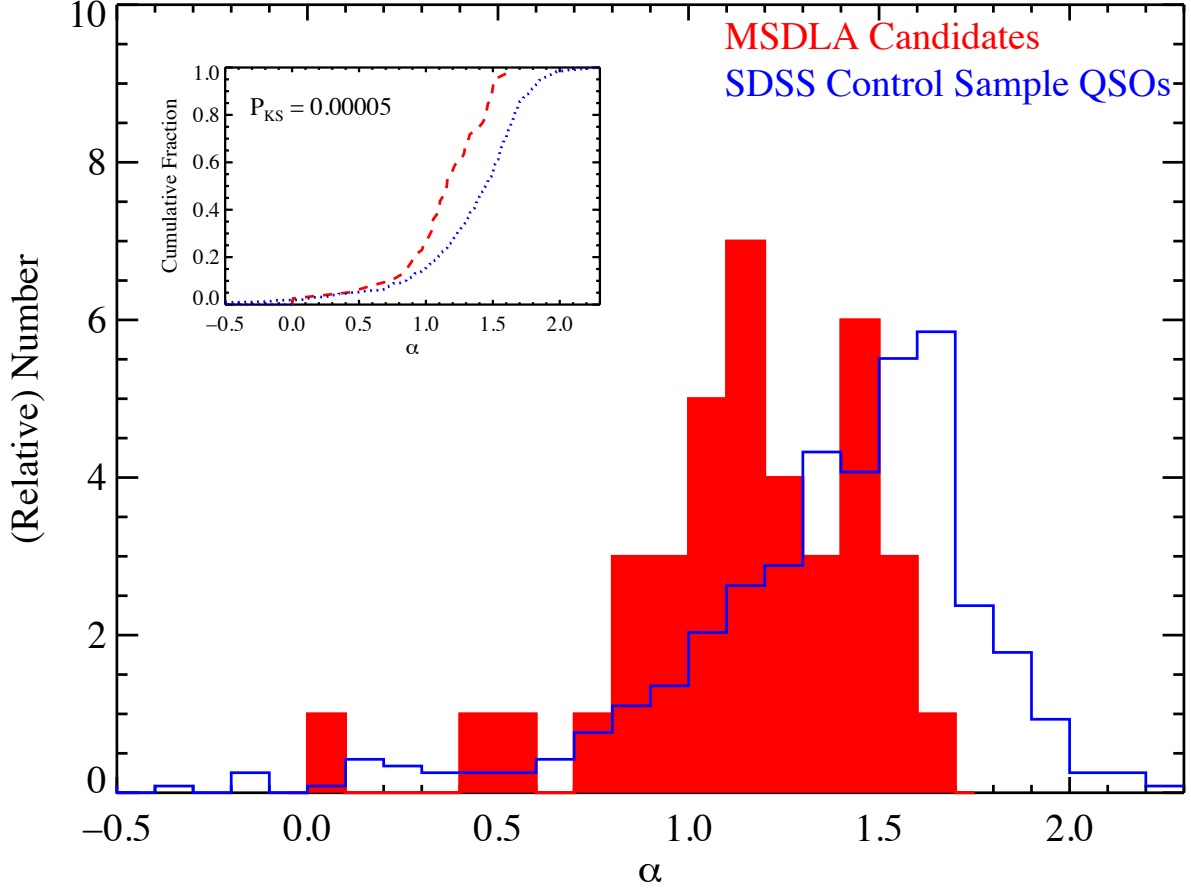
Fig. 7.— Histogram of power-law exponents (α) for the MSDLA candidates (red) compared against a control sample from the SDSS-DR5 taken to have the same r-magnitude and redshift distribution as the MSDLAs (normalized to have the same area under the curve). Larger α values indicate a bluer quasar spectrum. The upper left plot shows the normalized, cumulative distribution. The MSDLA candidates show systematically lower α values indicating reddening by dust within the galaxies. The difference in median α between the control sample and cMSDLAs is $\delta\alpha = 0.29$.

Table 3.   Calculated alpha and dust absorption parameters

QSO	z_{em}	z_{abs}	α_r	α_b	Dust Absorption (MMT)	Dust Absorption (SDSS)	$\log N_{\rm eff}^a$ $(\rm cm^{-2})$
J0008-0958	1.9512	1.7669	1.27	0.27	0.430 ± 0.490	...	20.57
J0016-0012	2.0869	1.9720	1.05	0.05	-0.011 ± 0.055	...	19.97
J0020+1534	1.7635	1.6521	1.16	0.16	...	...	19.84
J0044+0018	1.8677	1.7245	1.29	0.29	0.067 ± 0.141	...	19.64
J0058+0115	2.4949	2.0134	1.60	0.60	0.039 ± 0.110	0.034 ± 0.105	20.12
J0120+1324	2.5671	1.9998	1.50	0.50	-0.007 ± 0.227	0.076 ± 0.286	20.32
J0316+0040	2.9206	2.1805	0.98	-0.02	-0.027 ± 0.152	-0.037 ± 0.145	19.90
J0755+2342	1.8249	1.6702	1.29	0.29	0.062 ± 0.109	...	...
J0756+1648	2.8656	1.9730	1.05	0.05	-0.140 ± 0.124	-0.209 ± 0.070	...
J0812+3208	2.7105	2.6257	1.02	0.02	0.076 ± 0.129	0.056 ± 0.110	20.47
J0820+0819	2.5191	1.9545	1.22	0.22	-0.101 ± 0.049	-0.081 ± 0.060	...
J0831+4025	2.3300	2.0841	1.33	0.33	0.063 ± 0.225	0.117 ± 0.254	...
J0840+4942	2.0763	1.8502	0.97	-0.03	0.060 ± 0.236	...	20.32
J0856+3350	1.7256	1.6545	1.16	0.16	-0.193 ± -0.136	...	...
J0912-0047	2.8593	2.0710	1.49	0.49	-0.062 ± 0.153	-0.095 ± 0.128	20.43
J0927+5823	1.9100	1.6350	0.01	-0.99	-0.044 ± 0.011	...	20.18
J0938+3805	1.8274	1.8266	0.58	-0.42	-0.205 ± -0.147	...	...
J0958+4222	2.6558	2.0650	1.51	0.51	0.022 ± 0.120	0.053 ± 0.148	...
J1009+5450	2.0616	1.8922	1.09	0.09	0.172 ± 0.358	...	...
J1019+5246	2.1701	2.0181	1.43	0.43	0.094 ± 0.152	...	...
J1029+1039	1.7946	1.6221	1.04	0.04	0.135 ± 0.216	...	...
J1049-0110	2.1153	1.6580	1.13	0.13	-0.092 ± 0.012	...	19.61
J1054+0348	2.0947	2.0682	1.45	0.45	0.087 ± 0.144	...	...
J1056+1208	1.9227	1.6091	1.20	0.20	0.343 ± 0.420	...	21.04
J1057+1506	2.1690	2.0761	1.64	0.64	0.100 ± 0.158	...	...
J1111+1336	3.4816	3.2011	1.46	0.46	-0.141 ± -0.043	-0.162 ± -0.065	...
J1224+5525	1.8788	1.6727	1.45	0.45	0.118 ± 0.165	...	...
J1310+5424	1.9292	1.8004	0.43	-0.57	0.061 ± 0.151	...	20.96
J1312+5502	1.9065	1.8604	0.91	-0.09	0.362 ± 0.533	...	...
J1341+5818	2.0542	1.7407	1.10	0.10	0.111 ± 0.191	...	...
J1357+3450	2.9214	2.1316	0.86	-0.14	-0.059 ± 0.207	-0.068 ± 0.201	...
J1610+4724	3.2169	2.5078	1.15	0.15	0.201 ± 0.448	0.095 ± 0.375	21.02
J1709+3258	1.8891	1.8300	0.82	-0.18	0.062 ± 0.259	...	20.69
J2100-0641	3.1376	3.0920	1.50	0.50	0.128 ± 0.240	0.052 ± 0.173	20.38
J2123-0050	2.2623	2.0582	1.39	0.39	-0.028 ± 0.022	0.022 ± 0.065	...
J2125+0029	1.9505	1.7510	1.11	0.11	0.457 ± 0.563	...	...
J2222-0946	2.9263	2.3545	0.89	-0.11	-0.306 ± -0.204	-0.294 ± -0.193	19.94
J2244+1429	1.9546	1.8153	1.32	0.32	0.129 ± 0.284	...	19.81
J2340-0053	2.0845	2.0541	0.74	-0.26	0.135 ± 0.183	...	19.76

[a]Log effective column density defined as $\log N_{\rm HI} + [\rm M/H]$.

extinction (A_λ) and reddening (E_{B-V}).

Total extinction at a given wavelength is defined as:

$$A_\lambda = -2.5 \cdot \log_{10}\left[\frac{f_{obs}(\lambda)}{f_{intrinsic}(\lambda)}\right]. \qquad (2)$$

We also wish to constrain the reddening $E_{B-V} \equiv A_B - A_V$, but we do not have wavelength coverage of the B and V bands in the absorber rest frame. Instead, we take a reddening value in the ultraviolet $E_{\lambda_1-\lambda_2} \equiv A_{\lambda_1} - A_{\lambda_2}$ and then use an assumed extinction law ξ_λ to convert $E_{\lambda_1-\lambda_2}$ into E_{B-V}.

The control sample of QSOs with no absorption systems give an intrinsic flux $f_{intrinsic}(\lambda)$ where no light is absorbed by dust. The sample of cMSDLAs represent systems where flux is lost to dust absorption $f_{obs}(\lambda)$. We model the flux of the QSO continuum as the power-law seen in Eq. 1. For two wavelengths λ_1 and λ_2, the reddening $E_{\lambda_1-\lambda_2}$ may be written as

$$E_{\lambda_1-\lambda_2} \qquad = A_{\lambda_1} - A_{\lambda_2} \qquad (3)$$

$$(4)$$

$$= -2.5 \cdot log_{10}\left[\left(\tfrac{\lambda_1}{\lambda_2}\right)^{\delta\alpha}\right].$$

To evaluate the reddening, we set λ_1 and λ_2 to values representative of the emission-free windows in our analysis of the quasar continuum. The analysis typically covers $\approx 1300 - 2250$Å in the quasars' rest-frame. Converting from the median QSO redshift of $z_{em} = 2.087$ to the median absorber redshift of $z_{abs} = 1.955$ gives $\lambda_1 \approx 1390$Å and $\lambda_2 \approx 2400$Å. For $\delta\alpha = 0.29$, we infer $E_{\lambda_1-\lambda_2} \approx 0.17$ mag.

To convert to E_{B-V}, we must assume an extinction law. Observations to date suggest that DLAs exhibit SMC-like extinction (York et al. 2006; Wild & Hewett 2005) and we adopt this as our default extinction law (and test this assumption in the following sub-section). With the SMC law, we infer $E_{B-V} \approx 0.025$ mag and an average V-band extinction $A_V = E_{B-V} \cdot R_V \approx 0.076$ mag where we assumed $R_V = 3.1$. The latter is the favored value for the Galaxy, but also roughly holds for the SMC. This E_{B-V} value is systematically higher than any previously estimated for the DLAs (Murphy & Liske 2004; Ellison et al. 2005; Vladilo et al. 2008) as expected for a sample of absorbers pre-selected to have larger metal column densities.

With our predicted values for extinction and reddening, we can estimate the dust-to-gas ratio for the cMSDLAs. The cMSDLAs have a median H I column density of log $N_{\rm HI} = 20.85$ dex giving a median dust-to-gas ratio of $\log(A_V/N_{\rm HI}) \approx -22.0$ for the SMC

extinction law. We ignore the contribution of molecular hydrogen because it is expected to be a negligible contribution to the total amount of hydrogen (§ 4). A comparison to dust-to-gas ratios in the literature can be seen in Table 4. Our value for the dust-to-gas ratio of cMSDLAs is very similar to the SMC value $\log(A_V/N_{\mathrm{HI}}) = -22.1$ (Gordon et al. 2003), with a difference of only 0.1 dex. Vladilo et al. (2006) suggests that the dust-to-gas ratio scales with metallicity. We have metallicity values for 22 of the cMSDLAs, giving a median metallicity of $[\mathrm{M/H}] \approx -0.6$. This roughly follows the expected trend of dust-to-gas ratio vs. metallicity suggested by Vladilo et al. (2006). We conclude, therefore, that the dust-to-gas properties of the MSDLAs are generally consistent with that observed in the SMC. We also note that these inferences are subject to the assumed extinction law.

5.3.   The Possibility of the 2175 Å Bump

To test the assumption of an SMC-like extinction law, we have searched for the 2175 Å bump characteristic of a Galactic extinction law. The exact nature of the 2175 Å bump is unclear. It is thought to arise from the fine structure transitions of Polycyclic Aromatic Hydrocarbon (PHC) molecules in the Milky Way Galaxy (Allamandola & Hudgins 2003). The detection of the 2175 Å bump in the cMSDLAs would infer the existance of PHCs at high redshift (Wang et al. 2004). A visual inspection for a broad absorption feature at 2175 Å in the MMT spectra for each of the cMSDLAs yields no identifiable features. Malhotra (1997) was the first to attempt this sort of analysis. She created a composite spectrum of 96 Mg II absorbers and claimed a detection of the 2175 Å bump. Subsequent studies, however, have not confirmed this result (Ménard et al. 2005). Vladilo et al. (2008) and Vladilo et al. (2006) carried out similar searches using DLA samples. Vladilo et al. (2008) found no conclusive evidence for a 2175Å bump in their data while Vladilo et al. (2006) found evidence for a 2175Å bump in 1 out of 8 possible systems pre-selected to have very strong metal absorption. Although rare in DLAs, it is important to search for the 2175Å

Table 4.   Comparison of Dust-to-Gas Ratios

Object(s)	$\log(A_V/N_{HI})$	Reference
candidate MSDLAs	≈ -21.97	
SMC	$= -22.11$	Gordon et al. (2003)
Milky Way	$= -21.28$	Bohlin et al. (1978)
248 DLAs	≈ -22.53 to -22.40	Vladilo et al. (2008)

bump to test our use of an SMC-like extinction law. A composite spectrum of the cMSDLAs (shifted into the absorber rest frame) with a significantly higher signal-to noise ratio might yield evidence for a 2175 Å bump.

We constructed a composite spectrum of all our cMSDLAs by shifting each of their SDSS spectra into the DLA rest-frame, binning the pixels with 0.5 Å bins, and finding the weighted mean for all the pixels in each bin. We attempt to compensate for variation in the brightness of each QSO by having each individual spectrum scaled so that the median flux between 1000 and 1800 Å (QSO rest-frame) equals 100. The composite SDSS spectrum of the cMSDLAs can be seen in Fig. 8. Examining this composite spectrum does yield a possible broad absorption feature at ~ 2135 Å. This identification is questionable because of the high amount of irregularity in the continuum of the composite spectrum. This irregularity is caused by overlapping QSO broad emission lines from the individual spectra getting smeared out in the composite. The relatively low number of systems stacked in the composite spectrum is not enough to completely smooth out the emission lines intrinsic to the QSOs, where normally a composite of hundreds of systems would be needed. Two extinction law models are created, one for a MW-like extinction law and another for a SMC-like extinction law, which are overplotted with the composite cMSDLA spectrum. For each extinction model, a continuum is modeled with a power-law ($f \propto \lambda^{-\alpha}$) which is then artificially reddened with the respective extinction law to match the composite spectrum. These models can be seen in Fig. 8. The results of these fits are inconclusive. We conclude that the assumption of an SMC-like extinction law is justified although not required by our data.

5.4. Extinction Per Unit Column Density of Iron in Candidate MSDLAs

Previous works have asserted that gas in the DLAs and the ISM of local galaxies conforms to a nearly constant extinction per column density of metals in the dust phase (Vladilo et al. 2006). We can further explore this assertion with out sample of DLA systems. Specifically, the extinction per unit column density of iron in the dust phase, $\langle s_V^{Fe} \rangle$, is given by:

$$\langle s_V^{Fe} \rangle = \frac{A_V}{f_{Fe}\widehat{N}_{Fe}} \quad , \tag{5}$$

where $\widehat{N}_{Fe}$ is the dust phase column density of iron and f_{Fe} is the fraction of total iron atoms in the dust. The value of $\widehat{N}_{Fe}$ is often estimated by assuming Fe/Zn has an intrinsic, solar relative abundance, i.e. $\widehat{N}_{\mathrm{Fe}} = N_{\mathrm{Zn}}(\mathrm{Fe/Zn})_{\odot}$, assuming Zn has a negligible depletion into dust grains. If the extinction properties of dust are the same throughout the universe, one would expect that $\widehat{N}_{Fe} \propto A_V$ across a range of redshifts and metallicities. If this is true,
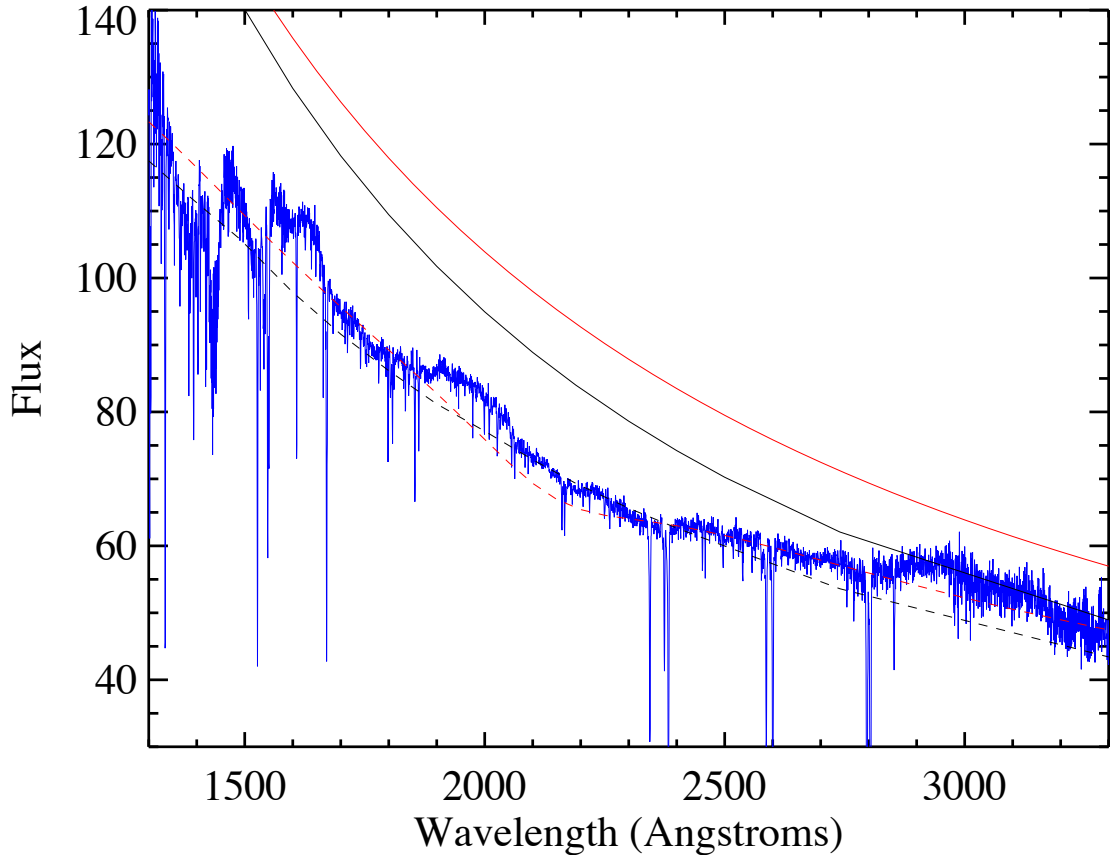
Fig. 8.— Composite spectrum of the cMSDLAs (blue). Two extinction-law models are overplotted, the SMC-like extinction law model (black) and the MW-like extinction law model (red) which contains the 2175Å bump. The solid lines above the composite spectrum are the power-law continua used for each model. The dotted lines overlapping the composite spectrum are the results of artificially reddening the continua. A possible broad absorption line feature is visible at ~ 2135 Å, but we are unable to confirm if this feature is genuine or caused by the variation in the composite spectrum's continuum. Therefore we claim no positive detection of the 2175Å bump.

then $\left\langle s_V^{Fe} \right\rangle$ is expected to be similar for any sight line, whether in our the Galaxy or in high redshift DLAs (Vladilo et al. 2006).

We proceed assuming a solar iron-to-zinc abundance ratio $\left(\frac{Fe}{Zn}\right)_\odot = 2.94$ (Asplund et al. 2009) for the cMSDLAs and that all of the iron is in the dust phase ($f_{Fe} = 1$). Of the 43 cMSDLAs, twenty-two have previous metallicity measurements with an average zinc column density of $\log N_{Zn} = \left[\frac{M}{H}\right] + \log N_{\mathrm{HI}} - 7.33 = 12.95$ dex. With $A_V \approx 0.076$ mag, we obtain $\left\langle s_V^{Fe} \right\rangle \approx 1 \times 10^{-17}$ mag cm^2 for the cMSDLA sample. This result is comparable to the value estimated by Vladilo et al. (2006) for a set of similar systems. It further supports their assertion that dust in the DLAs exhibits a roughly average extinction per column density of metals. In turn, this result stresses that the MSDLAs are excellent candidates to examining reddening by the ISM of high z galaxies.

5.5.   Dust Absorption for Individual Systems

While we have measured the average extinction and reddening of the cMSDLAs, we would like to measure absorption by dust in each individual system. This is challenging because the intrinsic QSO continua are unknown and likely exhibit large scatter. The previous analysis shows that α is depressed for the cMSDLAs and the power-law used to model the QSO continuum does provide a lower limit on the intrinsic flux which can be used. We use the previous power-law fits to extrapolate the QSO continuum further into the blue, specifically in the region between the QSO's Lyα and Lyβ emission lines. Departures from a strict power-law may indicate dust extinction and, in principle, could yield the extinction law for individual galaxies at far-UV wavelengths. In practice, however, our uncertainty on the intrinsic spectrum and (more importantly) absorption by the Lyα forest complicates the analysis. Nevertheless, this presents a test of our previous analysis from the power-law slopes measured outside the Lyα forest (§ 5.1).

The continuum of a QSO redward of ≈ 1300Å is well characterized by a single power-law $f_r(\lambda) \propto \lambda^{\alpha_r}$. In the far-UV, however, there is believed to be a break in this power-law to a second power-law $f_b(\lambda) \propto \lambda^{\alpha_b}$. We define the difference in exponents between these two power-laws as $\Delta\alpha \equiv \alpha_r - \alpha_b$. Composite QSO HST spectra by Telfer et al. (2002) gives $\Delta\alpha = 1.07 \pm 0.14$ with a break at ≈ 1250 Å. A similar analysis by Zheng et al. (1997) gives $\Delta\alpha = 0.97 \pm 0.16$ with a break at 1050 Å. For our analysis, we adopt a value of $\Delta\alpha = 1.0$ with a break at the QSO's Lyα emission line (1216 Å).

For each quasar, we create a model continuum by fitting to emission-free regions in the SDSS spectrum (§ 5.1). The shape of the continuum redward of 1216Å is described by

a power-law with the exponent α_r. This initial power-law breaks blueward of 1216Å and becomes a second power-law with $\alpha_b = \alpha_r - \Delta\alpha$, such as:

$$f_b(\lambda < 1216\text{Å}) = f(1216\text{Å})\left(\frac{\lambda}{1216\text{Å}}\right)^{-\alpha_b} \tag{6}$$

Our model QSO continuum is derived from the SDSS spectrum because it is assumed to have accurate flux and covers redder wavelengths where extinction is reduced. By extrapolating the model continuum into the blue, we aim to place a lower limit on the dust absorption in each system. We use the wavelengths between the QSO's Lyα and Lyβ emission lines to measure the dust absorption (1070 to 1170 Å). In this way the results are not contaminated by the QSO's emission lines. To estimate the contribution of the Lyα forest to the absorbed flux, we used values for the average absorption by the Lyα forest (DA) provided by Kirkman et al. (2005):

$$DA = 0.0062(1 + z)^{2.75}. \tag{7}$$

The flux in the region of extrapolated QSO continuum between the QSO's Lyα and Lyβ emission lines is then multiplied by DA to scale it down to the estimated flux after Lyα forest absorption. To avoid contamination from the DLA's Lyα absorption line, each line is individually masked out. Furthermore, the MMT spectrum blueward of 3190Å is avoided because of excessive noise. The mean flux of the Lyα to Lyβ region in both the SDSS and MMT spectra is then compared with the mean flux of the same region in the model continuum. If the mean flux of the model continuum is higher than the mean flux of the actual continuum, we attribute the lower than expected flux to absorption by dust in the DLA.

The fraction of observed flux compared to flux predicted by the model QSO continuum is termed d and is calculated as follows,

$$d = 1 - \frac{\overline{f}_{obs}(\lambda)}{\overline{f}_b(\lambda) \cdot (1 - DA)} \quad, \tag{8}$$

where $\overline{f}_{obs}$ is the average observed flux between 1070 and 1170Å and is defined as:

$$\overline{f}_{obs}(\lambda) = \frac{\sum_{i=1070\text{Å}}^{1170\text{Å}} f_{obs}^i(\lambda_{obs}) \cdot \Delta\lambda_{obs}^i}{\sum_{i=1070\text{Å}}^{1170\text{Å}} \Delta\lambda_{obs}^i} \quad. \tag{9}$$

Finally, $\overline{f}_b(\lambda)$ is the average flux of the model QSO continuum between 1070 to 1170 Å and is given by

$$\overline{f}_b(\lambda) = \frac{1}{\Delta\lambda} \int_{1070\text{Å}}^{1170\text{Å}} f_b(\lambda) d\lambda. \tag{10}$$

(1-DA) is the predicted fractional throughput of flux after absorption by the Lyα forest. The individual results for d can be seen in Table 3. If the parameter d truly scales with the amount of dust in a system, one would expect it is correlated with the system's measured metal column density.

For the latter, we introduce an effective column density $\log N_{\text{eff}} \equiv \log N_{\text{HI}} + [\text{M/H}]$ that characterizes the total metal column density for the absorber. We plot d vs. N_{eff} in Fig. 9. A regression line fit to the data gives a slope of 0.185 ± 0.046 (statistical error). A bootstrap analysis of 10,000 random samplings of the dataset indicates a positive slope at 95% confidence limit. The positive correlation between d and N_{eff} serves as evidence that MSDLAs contain detectable, if not significant, amounts of dust.

Future work will focus on these systems. By obtaining spectrophotometry from optical to near-IR wavelengths, we can constrain the intrinsic slope of the quasar and better estimate the underlying extinction law.

6. Summary and Concluding Remarks

We obtained MMT/BCS spectra of 41 QSO sightlines where previous observations found high metal column densities. We classify these absorption systems as candidate (c)MSDLAs. 49 absorbers with strong Lyα lines ($W > 5$Å) were identified, 43 of which correspond to the targeted cMSDLAs. The redshift for all absorption systems was determined visually by finding the centroid of low ion metal transitions. The H I column density ($\log N_{HI}$) for all absorption systems was measured by visually fitting a Voigt profile to the absorber's Lyα line. Out of 49 absorbers, 42 met the DLA criterion ($\log N_{HI} \geq 20.3$ atoms cm^{-2}) including all but two of the targeted cMSDLAs. The MSDLAs and cMSDLA show higher systematic H I column densities than comparable systems, in line with the expectation that selecting systems with high metal column density will also select systems with high H I column density.

Using the measured H I column densities and previously measured metal column densities, the metallicity [M/H] for each system was calculated. MSDLAs and cMSDLAs exhibit systematically higher metallicities than DLAs that are not metal strong. This suggests that MSDLA sightlines might probe towards the centers of galaxies where metallicity is greater, assuming a metallicity gradient. Perhaps MSDLAs represent a population of high redshift galaxies that became chemically enriched earlier in their evolution than others. Using these new calculations, we examined and extended the metallicity vs. Si II 1526 EW relation discussed by Prochaska et al. (2008). If this correlation is set by a underlying mass/metallicity relation, then the MSDLAs may represent the highest mass, gas-rich galaxies at high z.
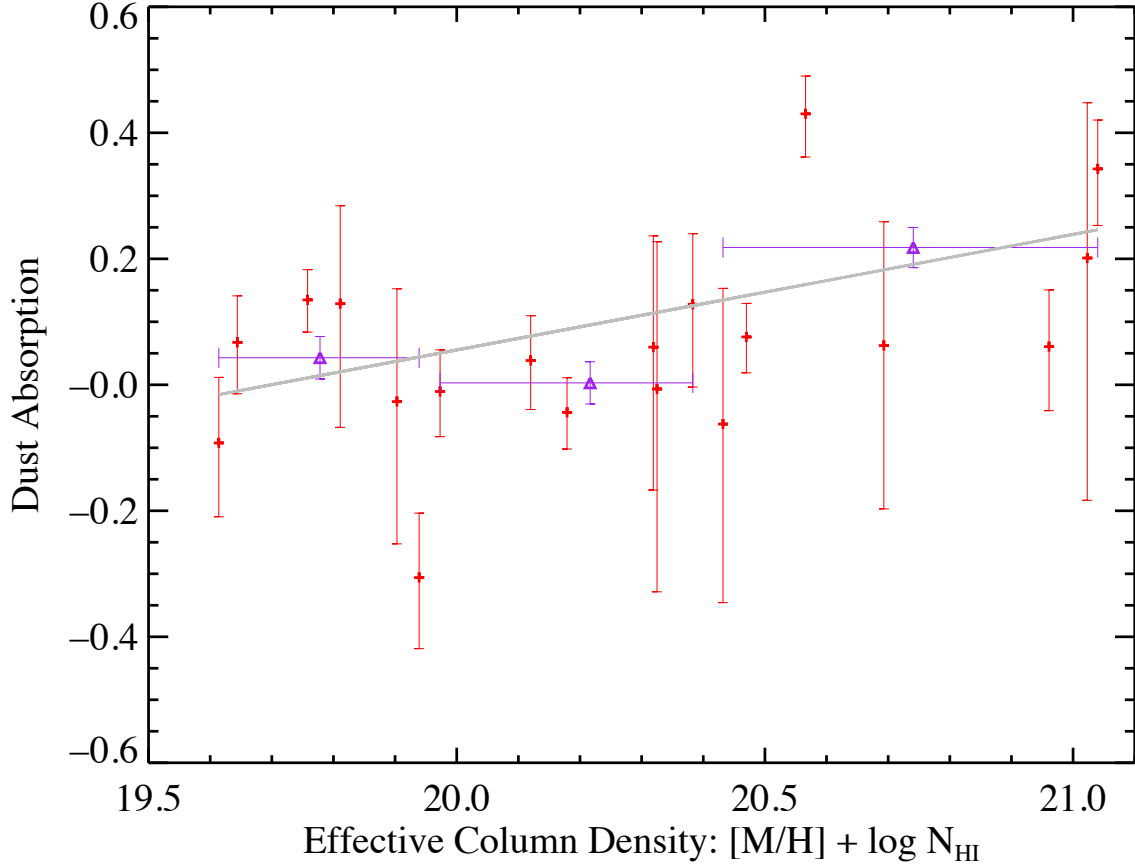
Fig. 9.— Dust absorption (as defined in the text) versus the effective column density of each cMSDLA with a measured metal column density and dust absorption value. Each of the three bins show the weighted mean of six DLAs. The regression line fit to the data has a slope of 0.185 ± 0.046. A bootstrap analysis of 10,000 random samplings of the dataset indicates a positive slope at 95% confidence limit, suggesting reddening from dust within the cMSDLAs in the far-UV. The purple points are bins that each represent the weighted mean of $\sim 1/3$ of the dataset.

We searched for signatures of dust in the cMSDLAs by studying the reddening of the background quasars. A power-law fit to the continuum of the SDSS spectra yielded individual power-laws (parameterized by α) that model the continuum of each QSO. The quasars behind cMSDLAs have lower α's then a control sample ($\delta\alpha = 0.29$) indicating significant extinction by dust in the cMSDLAs. Assuming an SMC-like extinction law, we estimate $A_V \approx 0.076\,\mathrm{mag}$ and $E_{B-V} \approx 0.025$ for these systems. The dust-to-gas ratio for the cMS-DLAs was estimated to be $\log(A_V/N_{HI}) \approx -22.0$, similar to the ratio for the SMC and roughly following the expected trend of the dust-to-gas ratio scaling with metallicity. The ratio of extinction to dust phase iron column density was estimated to be $\left\langle s_V^{Fe} \right\rangle \approx 1 \times 10^{-17}$.

The MSDLAs represent a unique subset of DLAs which are more chemically enriched, massive, dusty, and possibly evolved then ordinary DLAs. As such, they are excellent targets for future studies of extinction, nucleosynthesis, and searches for stellar light and molecular emission lines at high z.
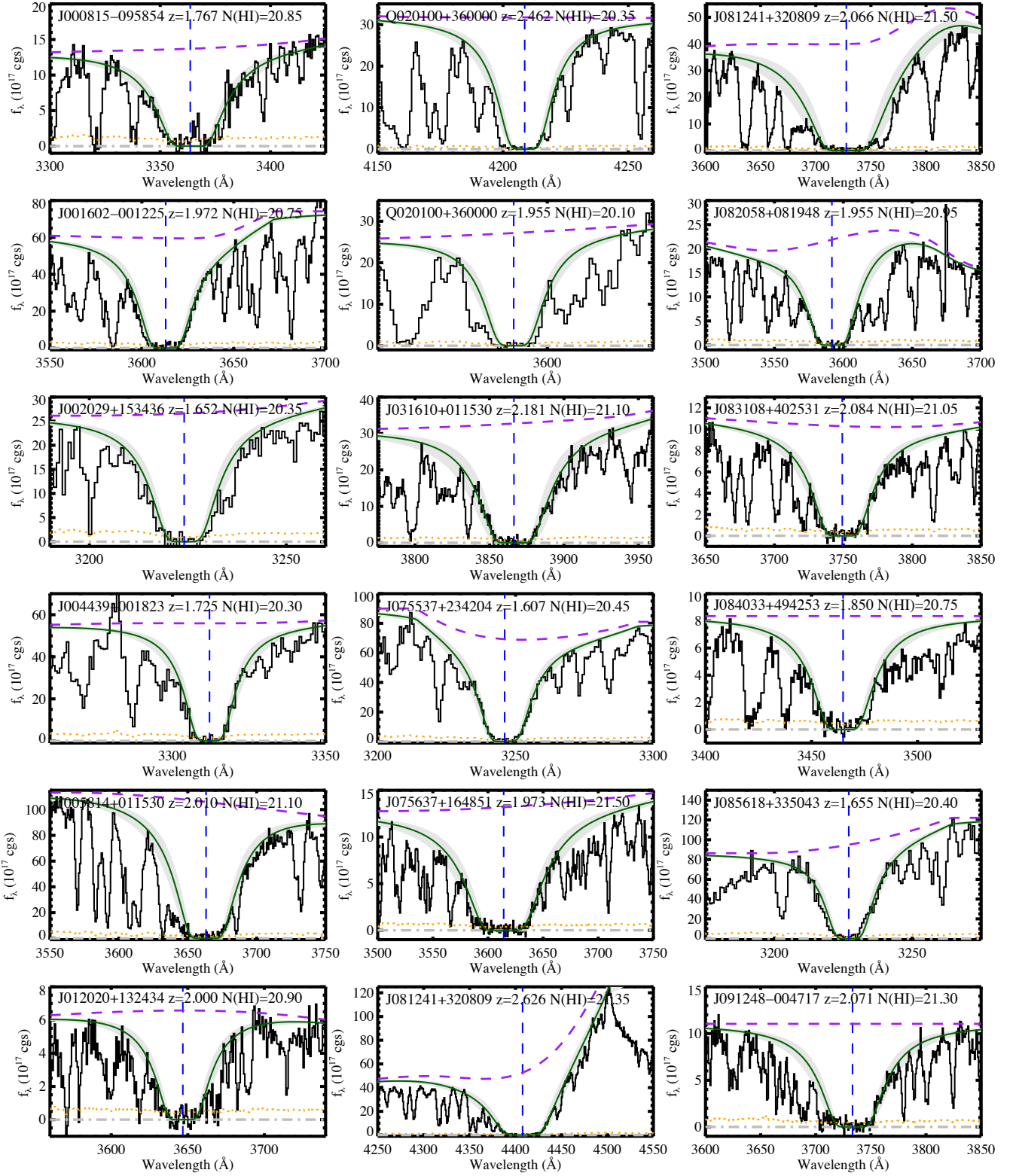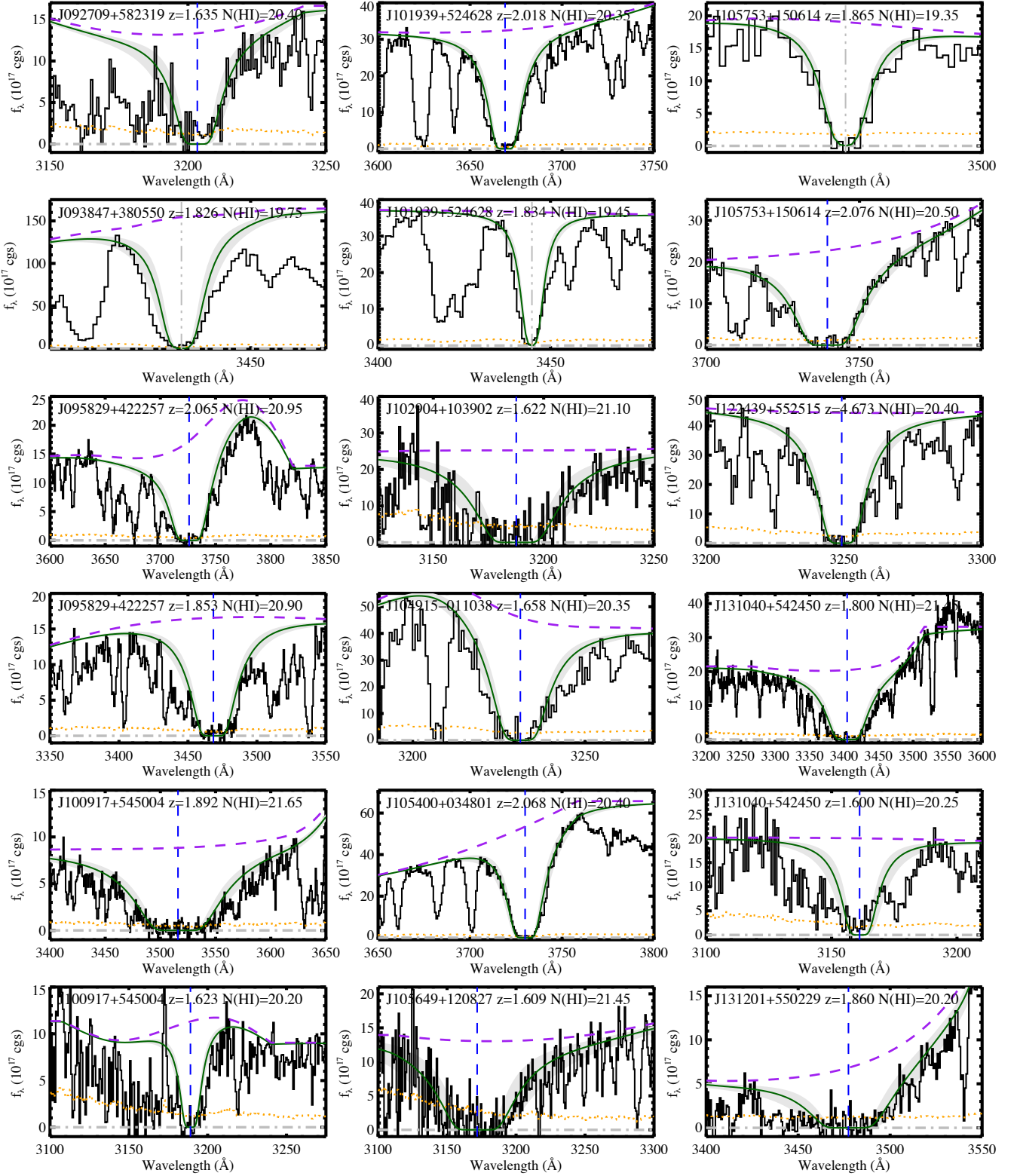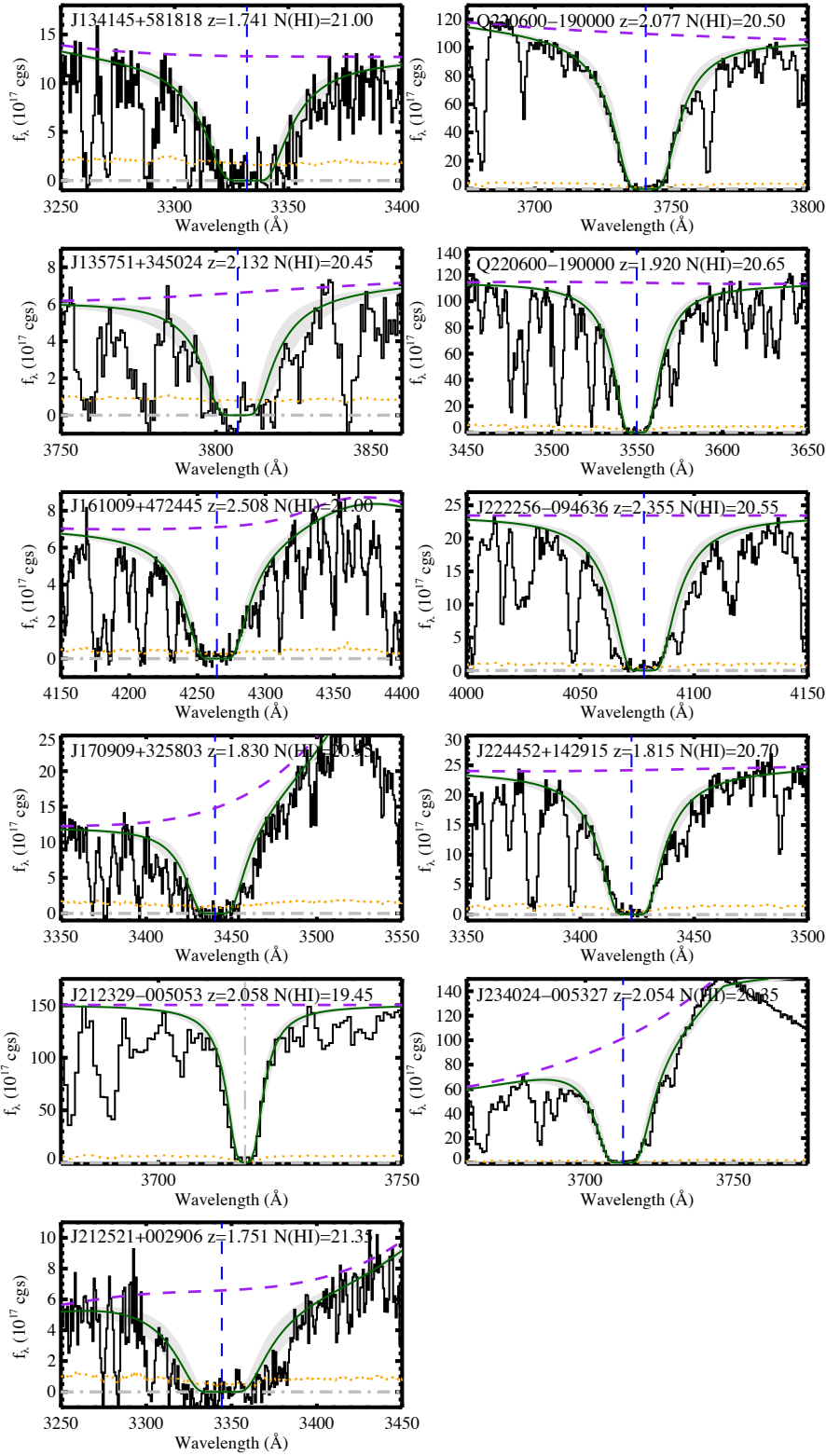
REFERENCES

Adelman-McCarthy, J. K., et al. 2008, ApJS, 175, 297

Allamandola, L. J., & Hudgins, D. M. 2003, in Solid State Astrochemistry, ed. V. Pirronello, J. Krelowski, & G. Manicò, 251–316

Asplund, M., Grevesse, N., Sauval, A. J., & Scott, P. 2009, ArXiv e-prints

Bohlin, R. C., Savage, B. D., & Drake, J. F. 1978, ApJ, 224, 132

Boisse, P., Le Brun, V., Bergeron, J., & Deharveng, J.-M. 1998, A&A, 333, 841

Ellison, S. L., Hall, P. B., & Lira, P. 2005, AJ, 130, 1345

Erb, D. K., Shapley, A. E., Pettini, M., Steidel, C. C., Reddy, N. A., & Adelberger, K. L. 2006, ApJ, 644, 813

Ge, J., & Bechtold, J. 1997, ApJ, 477, L73+

Gordon, K. D., Clayton, G. C., Misselt, K. A., Landolt, A. U., & Wolff, M. J. 2003, ApJ, 594, 279

Hamann, F., Kaplan, K. F., Rodriguez Hidalgo, P., Prochaska, J. X., & Herbert-Fort, S. 2008, ArXiv e-prints

Herbert-Fort, S., Prochaska, J. X., Dessauges-Zavadsky, M., Ellison, S. L., Howk, J. C., Wolfe, A. M., & Prochter, G. E. 2006, PASP, 118, 1077

Hubble, E. 1929, Proceedings of the National Academy of Science, 15, 3

Jenkins, E. B. 2009, ApJ, 700, 1299

Kirkman, D., et al. 2005, MNRAS, 360, 1373

Krumholz, M. R., Ellison, S. L., Prochaska, J. X., & Tumlinson, J. 2009, ApJ, 701, L12

Lu, L., Sargent, W. L. W., Barlow, T. A., Churchill, C. W., & Vogt, S. S. 1996, ApJS, 107, 475

Malhotra, S. 1997, ApJ, 488, L101+

Ménard, B., Zibetti, S., Nestor, D., & Turnshek, D. 2005, in IAU Colloq. 199: Probing Galaxies through Quasar Absorption Lines, ed. P. Williams, C.-G. Shu, & B. Menard, 86–91

Möller, P., Fynbo, J. P. U., & Fall, S. M. 2004, A&A, 422, L33

Murphy, M. T., Curran, S. J., Webb, J. K., Menager, H., & Zych, B. J. 2007, ArXiv Astrophysics e-prints

Murphy, M. T., & Liske, J. 2004, MNRAS, 354, L31

Nagamine, K., Springel, V., & Hernquist, L. 2004, MNRAS, 348, 421

Noterdaeme, P., Ledoux, C., Petitjean, P., & Srianand, R. 2008, A&A, 481, 327

O'Meara, J. M., Prochaska, J. X., Burles, S., Prochter, G., Bernstein, R. A., & Burgess, K. M. 2007, ApJ, 656, 666

Ostriker, J. P., & Heisler, J. 1984, ApJ, 278, 1

Pei, Y. C., Fall, S. M., & Bechtold, J. 1991, ApJ, 378, 6

Péroux, C., Kulkarni, V. P., Meiring, J., Ferlet, R., Khare, P., Lauroesch, J. T., Vladilo, G., & York, D. G. 2006, A&A, 450, 53

Petitjean, P., Srianand, R., & Ledoux, C. 2000, A&A, 364, L26

Pettini, M., Smith, L. J., Hunstead, R. W., & King, D. L. 1994, ApJ, 426, 79

Pontzen, A., et al. 2008, MNRAS, 390, 1349

Prochaska, J. X., Chen, H.-W., Wolfe, A. M., Dessauges-Zavadsky, M., & Bloom, J. S. 2008, ApJ, 672, 59

Prochaska, J. X., Gawiser, E., Wolfe, A. M., Castro, S., & Djorgovski, S. G. 2003a, ApJ, 595, L9

Prochaska, J. X., Gawiser, E., Wolfe, A. M., Cooke, J., & Gelino, D. 2003b, ApJS, 147, 227

Prochaska, J. X., Herbert-Fort, S., & Wolfe, A. M. 2005, ApJ, 635, 123

Prochaska, J. X., Howk, J. C., & Wolfe, A. M. 2003c, Nature, 423, 57

Prochaska, J. X., O'Meara, J. M., Herbert-Fort, S., Burles, S., Prochter, G. E., & Bernstein, R. A. 2006, ApJ, 648, L97

Prochaska, J. X., & Wolfe, A. M. 1996, ApJ, 470, 403

—. 2001, ApJ, 560, L33

—. 2009, ApJ, 696, 1543

Prochaska, J. X., Wolfe, A. M., Howk, J. C., Gawiser, E., Burles, S. M., & Cooke, J. 2007, ApJS, 171, 29

Prochaska, J. X., et al. 2001, ApJS, 137, 21

Savage, B. D., & Mathis, J. S. 1979, ARA&A, 17, 73

Savage, B. D., & Sembach, K. R. 1996, ARA&A, 34, 279

Telfer, R. C., Zheng, W., Kriss, G. A., & Davidsen, A. F. 2002, ApJ, 565, 773

Vladilo, G., Centurión, M., Levshakov, S. A., Péroux, C., Khare, P., Kulkarni, V. P., & York, D. G. 2006, A&A, 454, 151

Vladilo, G., Prochaska, J. X., & Wolfe, A. M. 2008, A&A, 478, 701

Wang, J., Hall, P. B., Ge, J., Li, A., & Schneider, D. P. 2004, ApJ, 609, 589

Wild, V., & Hewett, P. C. 2005, MNRAS, 361, L30

Wolfe, A. M., Gawiser, E., & Prochaska, J. X. 2005, ARA&A, 43, 861

York, D. G., et al. 2006, MNRAS, 367, 945

Zheng, W., Kriss, G. A., Telfer, R. C., Grimes, J. P., & Davidsen, A. F. 1997, ApJ, 475, 469